MASTER THESIS

Static and dynamic properties of a few interacting fermions trapped in an harmonic potential

Author
Abel Rojo Francàs

Supervisor
Dr. Artur Polls Martí
Dr. Bruno Julià Díaz

December, 2019

UNIVERSITAT DE
BARCELONA

TABLE OF CONTENTS

ACKNOWLEDGEMENTS

First of all, I would like to thank my supervisors, Artur and Bruno, for their support and advice in the realization of this thesis, as well as for the opportunities to attend seminars and conferences. It has been a pleasure to work with them, and I have been able to learn a lot from their teachings. I also want to thank my family and friends for all the support received during this time.

INTRODUCTION

The quantum many-body problem has long been of great interest as it has direct consequences for a large number of branches of science, from quantum chemistry, to condensed matter, high energy physics, nuclear physics and astrophysics. Well known examples are the electrons in a metal [1], the quark gluon plasma [2], nuclei or even nucleon stars [3]. In all these examples the physical properties of the system are a consequence of the fact of having a number of interacting quantum constituents.

Despite its importance, clearly recognized by the community, the quantum many-body problem always dealt with systems which were notably difficult to prepare and control. For instance, in the previous examples the interactions among the constituents are given by nature, and it is not feasible to produce artificial systems which are prone to be studied in detail, e.g. building laboratory neutron stars is nowadays unthinkable.

In recent years, the breakthroughs in the field of ultracold atomic gases have completely changed the situation. Soon after the experimental production of Bose-Einstein condensates [4, 5], the community shifted gears to trap and control not only bosonic atoms but also fermionic ones, mixtures of bosons, and of bosons and fermions [6–8]. This alone would already be a revolution, as it allows one to study for in the laboratory quantum particles which could only be studied in very intricate environments. On top of this, ultracold atomic experiments can nowadays also routinely vary the atom-atom interaction strength by means of Feshbach resonances and can also modify the trapping potential holding the particles [9–11], changing from quasi 1D or 2D setups to different geometries in 3D [12]. In recent years also species with a sizeable long range interaction have been produced, thus opening the door to the study of long-range interacting many-body systems [13]. From this point of view ultracold atomic systems are considered excel-

lent laboratories where condensed matter systems can be quantum simulated [14, 15].

In this work, we study a system with few spin 1/2 fermions in a one dimensional harmonic trap. The interaction between the fermions is modeled by a contact potential. In the literature exist some studies under similar conditions [16–18]. We study static and dynamic properties of few-fermion systems as a function of the interaction strength.

The structure of this work is the following. In Chapter 2, we present the theoretical description of the fermionic mixture considered. In particular, we write down the full Hamiltonian both in first and second quantized form. Some limiting scenarios are considered, e.g. zero interaction. In Chapter 3, we describe the numerical tools used to study the ground state and first excited states of the fermionic mixture. The main method employed is exact diagonalization of the Hamiltonian matrix in a truncated Hilbert space. In Chapter 4, we study the ground state of the system for several number of fermions and polarizations. In Chapter 5 we turn our attention to the lower part of the spectrum, computing the spectra for the same few-fermion systems considered. In Chapter 6, we study the response of the system to external perturbations. Finally in Chapter 7 we list the main conclusions of our work.

In this chapter we introduce the theoretical tools to describe a system of a few fermions trapped in a one dimensional harmonic oscillator potential.

2.1   The Hamiltonian of the system

We consider a system with a few fermions trapped in a one dimensional harmonic oscillator potential. In the first step, we define the Hamiltonian describing the system. The Hamiltonian is splitted in two parts, one part describes the particles in a harmonic oscillator potential, and the other takes care of the interactions between the fermions. Therefore, the Hamiltonian can be written as [18, 19]

$$(2.1.1) \qquad H = \sum_{i=1}^{N} H_{\text{ho}} + \sum_{j<i}^{N} V_{\text{int}}(x_i - x_j).$$

The harmonic oscillator Hamiltonian, H_{ho}, is a one body operator and includes the kinetic and the harmonic potential energy. The 1D harmonic oscillator Hamiltonian reads,

$$(2.1.2) \qquad H_{\text{ho}} = -\frac{\hbar^2}{2m}\frac{\partial^2}{\partial x^2} + \frac{1}{2}m\omega^2 x^2,$$

where m is the particle mass and ω is the frequency of the harmonic oscillator. The eigenvalues of this Hamiltonian are,

$$(2.1.3) \qquad E_n = \left(n + \frac{1}{2}\right)\hbar\omega \quad n = 0, 1, 2, \ldots,$$

and the corresponding eigenfunctions are written as,

$$(2.1.4) \qquad \Phi_n(x) = \frac{1}{\sqrt{2^n n!}}\left(\frac{m\omega}{\pi\hbar}\right)^{1/4} e^{-\frac{m\omega x^2}{2\hbar}} H_n\left(\sqrt{\frac{m\omega}{\hbar}}x\right),$$

3

where $H_n(x)$ is the n-th Hermite polynomial. These functions will be used to build the many-body basis. All these functions have a similar structure: a Gaussian function multiplied by an Hermite polynomial with a normalization factor, that depends on n.

We consider identical fermions of spin 1/2, i.e., with two possible spin states: $|1/2, m\rangle$, $m = 1/2, -1/2$, which sometimes will be denoted by: $|\uparrow\rangle$ and $|\downarrow\rangle$, respectively. The fermions are assumed to interact via a contact delta potential [20]. Therefore two fermions interact only if they are at the same position. However, the many-body wave function of a system of identical fermions should be antisymmetric, preventing two fermions with the same spin to occupy the same position. Therefore the fermions with the same spin projection do not interact and the interaction is active only between fermions with different spin projection.

In any case, the total wave function including the spin degree of freedom should be antisymmetric. This requirement allows to have two particles with different spin projection in the same position.

The interaction term of Eq. (2.1.1) is a contact interaction, which is expressed as [21]

$$(2.1.5) \qquad V_{\text{int}}(x_i - x_j) = g\delta(x_i - x_j),$$

where g characterizes the strength of the interaction and δ is a Dirac delta function.

Taking into account the identity [22]

$$(2.1.6) \qquad \sum_{i=1}^{N} x_i^2 = NX^2 + \frac{1}{N}\sum_{i<j}(x_i - x_j)^2,$$

where $X = \frac{1}{N}\sum_i x_i$ is the center of mass coordinate, the Hamiltonian can be splitted in two pieces

$$(2.1.7) \qquad H = H_{\text{CM}} + H_{\text{r}},$$

where H_{CM} in harmonic oscillator units reads:

$$(2.1.8) \qquad H_{CM} = -\frac{1}{2N}\frac{d^2}{dX^2} + \frac{N}{2}X^2,$$

describes the center of mass motion and H_r affects only the relative coordinates and is translationally invariant.

One way to create a one dimensional trap is using a cigar shaped trapping potential, with the transverse trap frequency $\omega_\perp$ (in the radial direction) much higher than the trap frequency ω in the axial direction. In this situation, the coupling constant g is related to the one dimensional scattering length ($a_{1\text{d}}$) as [9, 20],

$$(2.1.9) \qquad g = -\frac{\hbar^2}{ma_{1\text{d}}}.$$

From the relation between the one-dimensional scattering length and the three-dimensional scattering length [23], we can write the coupling constant as

$$(2.1.10) \qquad g = \frac{2\hbar^2 a_{3d}}{m a_\perp^2} \frac{1}{1 - |\xi(1/2)| a_{3d}/(\sqrt{2} a_\perp)},$$

with $a_\perp = \sqrt{\hbar/m\omega_\perp}$ and ξ is the Riemann zeta function.

In a trap under these conditions, the system can be treated as a one dimensional system. As the trapping in the transverse dimension is very strong, all particles occupy the lowest state of the transverse harmonic oscillator and the physics takes place in the longitudinal direction [23].

For convenience we will use the harmonic oscillator units, in which the energy is measured in $\hbar\omega$ units, the length in units of $\sqrt{\hbar/m\omega}$ and the coupling constant g is expressed in units of $\sqrt{m}/\sqrt{\omega\hbar^3}$. From this moment on, all magnitudes will be expressed in these units.

2.2 Non-interacting and infinite interaction limits

In general, it is not possible to solve analytically the Schrödinger equation for a given value of the interaction strength. However, there are two limits: the non-interacting and the infinite interaction cases for which one has an explicit analytical solution [24].

For these two limits, we can easily determine the energy and the density profile of the ground state of the system, and explicitly write the wave function.

2.2.1 Non-interacting case: Fermi gas

In the non-interacting case, the system is in a state called Fermi gas. In these conditions, the behavior of the system is given by the single-particle states of the harmonic oscillator with the restriction of the Pauli principle that does not allow to have two fermions with the same spin projection in the same harmonic oscillator state. More specifically, in the ground state of a system with N_d particles of spin down and N_u particles of spin up, the particles occupy the lowest single-particle energy states, N_d and N_u respectively. Therefore, the energy of the ground state is

$$(2.2.1) \qquad E_{gs}(g=0) = \sum_{n=0}^{N_d-1} \left(n + \frac{1}{2}\right) + \sum_{n=0}^{N_u-1} \left(n + \frac{1}{2}\right) = \frac{N_d^2 + N_u^2}{2}.$$

Actually the wave function of the system is given by a Slater determinant built with the lowest N_u and N_d single particle wave functions with spin up and down respectively.

The total third component of the spin of this wave function is $M = \frac{N_u - N_d}{2}$ and the total spin is the minimum S compatible with M, $S = M$ [25].

The density profile associated to this wave function will be the sum of the probabilities of finding a particle in each occupied state in the position x,

$$(2.2.2) \qquad \rho(x) = \sum_{n=0}^{N_d-1} |\Phi_n(x)|^2 + \sum_{n=0}^{N_u-1} |\Phi_n(x)|^2 ,$$

where $\Phi_n(x)$ are the 1D harmonic oscillator wave functions. The density profile is normalized to the number of particles.

2.2.2 Infinite interaction case: Tonks-Girardeau gas

In the infinite interaction limit, the system experiences a phenomenon similar to the fermionization process in Bose systems. In fact, the bosons under this situation, are described as a system of non-interacting identical fermions [18]. This system is known as a Tonks-Girardeau gas. In our case, the wave function can be written as [24],

$$(2.2.3) \qquad \Psi = \Psi_A \Psi_S ,$$

where Ψ_A is an antisymmetric wave function on the spatial coordinates and Ψ_S is a symmetric wave function with depends on both spatial and spin coordinates. The antisymmetric part, Ψ_A, is a Slater determinant built with the $N = N_d + N_u$ harmonic oscillator wave functions. And the symmetric part, Ψ_S, is a linear combination of products of sign functions of differences of the particle coordinates and their spin functions. The energy of the ground state depends only on the single-particle states present in Ψ_A is

$$(2.2.4) \qquad E_{\text{gs}}(g \to \infty) = \sum_{n=0}^{N-1} \left(n + \frac{1}{2} \right) = \frac{(N_d + N_u)^2}{2} .$$

The different Ψ_S functions associated with the same Ψ_A define the degeneracy of the ground state: $D = \frac{N!}{N_u! N_d!}$ [24].

The total third spin component of this wave function is $M = \frac{N_u - N_d}{2}$. However, different total spin functions coexist in the degenerated ground state.

The density profile associated to this wave function will be the sum of the probabilities of finding a particle in each occupied state in the position x,

$$(2.2.5) \qquad \rho(x) = \sum_{n=0}^{N-1} |\Phi_n(x)|^2 ,$$

where $\Phi_n(x)$ are the 1D harmonic oscillator wave functions.

2.3 Second quantization

When working with several particles, it is useful to use the second-quantization formalism. This formalism is based on the occupation number of the single-particles states. In order to define the Fock space, we need to have a single-particle basis, such as the harmonic oscillator states. The basis of the Fock space is constructed by indicating how many particles occupied each single-particle state. In addition, the rules of antisymmetry are implemented by the anticommutation rules fulfilled by the creation and annihilation operators [26].

A particular state is the vacuum state denoted by $|0\rangle$. This vector represents a state without particles, i.e., all its occupation numbers are zero. This state has norm equal to 1.

2.3.1 Creation and annihilation operators

The main tool in second quantization are the creation and annihilation operators, which act on the Fock space. These operators are important because any operator can be expressed in term of them [26].

The action of a creation operator on the vacuum state, denoted as $a_i^\dagger |0\rangle$, creates a particle in the state i. In general, in applying a creation operator on a Fock space vector, creates a particle in the i state, whenever possible. Or in other words, it increases the occupation number of this single-particle state by one.

In general, the action of an annihilation operator on a state destroys a particle in the i state, whenever possible. In other words, it decreases the occupation number of the state by one.

Also, a Fock space vector with N particles can be created by the action of N creation operators on the vacuum space, as follows,

$$|n_1, n_2, n_3, ..., n_m\rangle = (a_1^\dagger)^{n_1}(a_2^\dagger)^{n_2}(a_3^\dagger)^{n_3}...(a_m^\dagger)^{n_m}|0\rangle \tag{2.3.1}$$

with $N = \sum_i n_i$.

In the case of fermions, to satisfy the Pauli principle, i.e., the antisymmetry of the wave function, the creation and annihilation operators should fulfill the following anti-commutation relations

$$\left\{a_i^\dagger, a_j\right\} = \delta_{ij}$$
$$\left\{a_i^\dagger, a_j^\dagger\right\} = \left\{a_i, a_j\right\} = 0. \tag{2.3.2}$$

Therefore the occupation number of the Fock basis can take the values $n_i = 0$ or $n_i = 1$. Then, the

creation and annihilation operators must also fulfill these conditions and respect normalization. Finally, the action of creation (annihilation) operator can be written as

(2.3.3)
$$a_i^\dagger |n_1, n_2, ... n_{i-1}, n_i, ...\rangle = (-1)^{N_i} \sqrt{1 - n_i} |n_1, n_2, ... n_{i-1}, (1 - n_i), ...\rangle$$
$$a_i |n_1, n_2, ... n_{i-1}, n_i, ...\rangle = (-1)^{N_i} \sqrt{n_i} |n_1, n_2, ... n_{i-1}, (1 - n_i), ...\rangle ,$$

where N_i is the number of occupied states with index lower than i,

(2.3.4)
$$N_i = \sum_{k=1}^{i-1} n_k .$$

The phase $(-1)^{N_i}$ is due to the anti-commutation relations. Notice that the factor in front of the state becomes zero if one tries to put two particles in the same single-particle state or one tries to annihilate a particle in a single-particle state not occupied.

2.3.2 Fock space

The harmonic oscillator eigenfunctions are used to build the many-body basis of the Fock space. In addition, the spin degrees of freedom are also incorporated to the single particle wave functions which are defined as: $\Psi_{n,m}(x,s) = \Phi_n(x)\chi_m(s)$, where $\Phi_n(x)$ is the harmonic oscillator wave function of the level n and χ_m is the spin wave function, where $m = \uparrow (\downarrow)$ is the spin projection.

With these single-particle states, we build the many-body basis of the Fock space:

(2.3.5)
$$\left| n_{0\downarrow}, n_{0\uparrow}, n_{1\downarrow}, n_{1\uparrow}, ... \right\rangle ,$$

where $n_{i,m}$ indicates the number of particles in the $\Psi_{i,m}$ single-particle state.

2.3.3 Operators in second quantization

In second quantization, the operators can be expressed in terms of creation and annihilation operators.

A general one-body operator $\hat{\mathscr{O}}$ in second quantization is expressed as

(2.3.6)
$$\hat{\mathscr{O}} = \sum_{i,j} \langle i| \hat{O} |j\rangle a_i^\dagger a_j ,$$

where $|i\rangle$ and $|j\rangle$ are single-particle states and $\langle i| \hat{O} |j\rangle = \int \varphi_i^*(x) O(x) \varphi_j(x) dx$ is the one-body matrix element and $\varphi_i(x)$ are the single-particle wave functions.

A general two-body operator $\hat{\mathscr{V}}$ in second quantization is expressed as

(2.3.7)
$$\hat{\mathscr{V}} = \frac{1}{2} \sum_{i,j,k,l} \langle i,j| \hat{V} |k,l\rangle a_i^\dagger a_j^\dagger a_l a_k = \frac{1}{2} \sum_{i,j,k,l} v_{ij,kl} a_i^\dagger a_j^\dagger a_l a_k ,$$

where $v_{ij,kl}$ is the two-body matrix element defined as

(2.3.8)
$$v_{ij,kl} = \int \varphi_i^*(x_1) \varphi_j^*(x_2) \mathscr{V}(x_1, x_2) \varphi_k(x_1) \varphi_l(x_2) dx_1 dx_2 .$$

2.3.4 The Hamiltonian in second quantization

As already mentioned, the Hamiltonian describing the harmonic oscillator is a one-body operator. On the other hand, the interaction term Eq. (2.1.1) is a two-body operator. In our case, choosing a harmonic oscillator eigenfunctions as the single-particle basis, the Hamiltonian part corresponding to the harmonic oscillator is diagonal, with eigenvalues $\epsilon_i = i + 1/2$. Therefore in second quantization it will be expressed as

$$(2.3.9) \qquad \hat{H}_{\mathrm{ho}} = \sum_{i,j} \langle i | H_{\mathrm{ho}} | j \rangle a_i^\dagger a_j = \sum_{i,j} \epsilon_i \delta_{i,j} a_i^\dagger a_n = \sum_i \epsilon_i a_i^\dagger a_i = \sum_i \epsilon_i \hat{n}_i \,,$$

where $\hat{n}_i = a_i^\dagger a_i$ is the number operator associated to the single particle state $|i\rangle$.

For the interaction term, we express its interaction matrix elements as

$$
\begin{aligned}
v_{ij,kl} &= \int dx_1 dx_2 \Psi_{i,m_i}^*(x_1, s_1) \Psi_{j,m_j}^*(x_2, s_2) g\delta(x_1 - x_2) \Psi_{k,m_k}(x_1, s_k) \Psi_{l,m_l}(x_2, s_l) \\
(2.3.10) \qquad &= g \int dx \Phi_i^*(x) \Phi_j^*(x) \Phi_k(x) \Phi_l(x) \langle \chi_{m_i} \chi_{m_j} | \chi_{m_k} \chi_{m_l} \rangle \\
&= g\delta_{m_i,m_k} \delta_{m_j,m_l} \int dx \Phi_i^*(x) \Phi_j^*(x) \Phi_k(x) \Phi_l(x).
\end{aligned}
$$

Notice that the interaction does not affect the spin of the particles, and we have used the orthogonality of the spin functions: $\langle \chi_{m_i} \chi_{m_j} | \chi_{m_k} \chi_{m_l} \rangle = \delta_{m_i,m_k} \delta_{m_j,m_l}$. The calculation of the integral can be found in Appendix A.

Finally, the Hamiltonian reads

$$(2.3.11) \qquad H = \sum_i \hat{n}_i \epsilon_i + \frac{1}{2} \sum_{ijkl} v_{ij,kl} a_i^\dagger a_j^\dagger a_l a_k \,.$$

3

NUMERICAL METHODS

In this chapter we present the method named exact diagonalization used to solve the many-body Schrödinger equation. The technical aspects on how to construct the matrix Hamiltonian, to choose a suitable many-body basis of the Fock space, and how to calculate the two-body matrix elements are discussed in detail. Finally, we use the two-particle system, that has an analytical solution [27], as a benchmark of our numerical procedure.

3.1 Exact diagonalization

In order to study the ground state and the low-excited states of a system, one has to solve the many-body Schrödinger equation. With this objective, we use an exact diagonalization method. This method needs to built the Hamiltonian matrix in an appropriate subspace and diagonalize it. In order to obtain accurate results we need to use a large basis, generating large matrices. To diagonalize these large matrices, we use a Lanczos method implemented by the ARPACK package [28]. This method allows to diagonalize large matrices, and obtain the lowest eigenvalues with high accuracy.

With the exact diagonalization method, one obtains the energy spectrum and the corresponding eigenstates. However if we want the exact state and its energy, we need to use the complete Hilbert space, in this case, with an infinite basis. Notice, that in any case the results using a Hilbert subspace are always variational.

3.2   Particle configurations

We consider systems with two, three, four and five particles. These particles have spin 1/2, therefore for N particles we can have $N + 1$ possible total spin projections. As the Hamiltonian commutes with the total third spin component, the Hamiltonian is built in boxes with well defined M. Thus, it is possible to treat each total spin projection independently [18]. The simplest case is when all fermions have spin up, then $M = N/2$, and the wave function factorizes in a antisymmetric spatial wave function and a symmetric spin wave function $\chi(S = N/2, M = N/2)$ for N particles. The antisymmetric spatial wave function is a Slater determinant built with the lowest single particle states. The antisymmetry of the wave function prevents two particles being in the same position and the particles in this wave function do not feel the contact interaction. Therefore, its energy is independent of the interaction strength.

The other trivial cases are the negative M values because due to the spin symmetry of the Hamiltonian, the properties of the states do not depend on the sign of the spin projection. The diagonalization of a Hamiltonian box with a given M would provide the same eigenvalues that the box with total spin projection $-M$. Therefore we will concentrate in the study of the following cases: the system with $N = 2$ with total spin projection $M = 0$. Next we explore the systems with $N = 3$ and total spin projection $M = 1/2$, and the two systems with $N = 4$ and $M = 0$ and $M = 1$. Finally, we study also the systems with $N = 5$ and $M = 1/2$ and $M = 3/2$.

3.3   Basis truncation

To obtain the exact results, when using a diagonalization method, we would need to use the complete basis. However this is not possible because of the infinite dimension of the Hilbert space. Therefore we are forced to diagonalize the Hamiltonian in a finite subspace. Usually, this procedure does not provide the exact eigenvalue. However, the lowest energy obtained by diagonalization is still an upper-bound to the ground state energy.

A common way to construct a finite many-body basis is considering a finite number of single-particle states, usually, those with the lowest energy [29].

In our case, we diagonalize the Hamiltonian in a subspace with well defined total third spin component. We start considering the lowest N_M single-particle states and take into account an energy constrain in the construction of the many-body basis: the energy of the many-body basis states, which is given by the sum of the single-particle energies, should be smaller or equal than a fixed energy $E_{\max}$ [30].

This maximum energy depends on the number of particles and spin configuration. Notice that we

	number of single-particle states	number of many-body basis states	
		with energy restriction	without restriction
2 particles, M=0	100	5,050	10,000
3 particles, M=1/2	50	10,725	61,250
4 particles, M=0	40	30,800	608,400
4 particles, M=1	40	19,530	395,200
5 particles, M=1/2	30	22,923	1,766,100
5 particles, M=3/2	30	11,349	822,150

Table 3.1: Number of single-particle states used in the construction of the many-body basis states in the second column. The number of many-body basis states, with and without energy restriction, are shown in columns third and fourth respectively.

consider always $M > 0$ therefore, $N_u > N_d$. The maximum energy, $E_{\max}$, corresponds to the energy of a non-interacting many-body state build as follows: one spin-up particle in the maximum single-particle energy state and the remaining $(N_u - 1)$ spin-up particles in the lowest $N_u - 1$ single-particle states. On the other hand the N_d spin-down particles are located in the lowest N_d single-particle states. Therefore, the maximum energy considered in the construction of the many-body basis is

$$(3.3.1) \quad E_{\max} = \sum_{n=0}^{N_d-1} \left(n + \frac{1}{2}\right) + \sum_{n=0}^{N_u-2} \left(n + \frac{1}{2}\right) + \left((N_M - 1) + \frac{1}{2}\right) = \frac{(N_d)^2 + (N_u - 1)^2}{2} + \left(N_M - \frac{1}{2}\right),$$

where N_M is the number of single-particle states used.

One can see in Table 3.1 that the dimension of the many-body basis is strongly reduced if the energy restriction discussed above is taking into account. Nevertheless, the reduction of the size of the space considered does not affect the quality of the results in the low energy regime of the spectrum. Note that the dimension of the many-body basis in the case without energy restriction is $\frac{(N_M)!}{(N_M - N_u)!N_u!} \frac{(N_M)!}{(N_M - N_d)!N_d!}$ which grows very rapidly.

3.4 Numerical calculation of the interaction matrix elements

The presence of factorials in the analytical expression of the matrix elements Eq. (A.0.8), given in the appendix, can originate numerical problems. In this section we propose a procedure to overcome this problem.

In general the matrix elements of the interaction should be well behaved. However, the presence of factorials in the expressions of the harmonic oscillator wave functions can originate fake overflows in the calculation. One possible solution to this problem is by taking logarithms of the expressions to be evaluated.

As it is shown in the appendix, a suitable way to write the integrals entering in the two-body matrix elements is

(3.4.1)
$$I_{abcd} = \sum_{r=0}^{d} \frac{1}{\pi^2 \sqrt{2}} \sqrt{\frac{c!d!}{a!b!}} \frac{1}{r!(d-r)!(c-d+r)!} \Gamma\left(\frac{a+b-c+d+1}{2} - r\right)$$
$$\times \Gamma\left(\frac{a-b+c-d+1}{2} + r\right) \Gamma\left(\frac{-a+b+c-d+1}{2} + r\right).$$

This expression can be written as $I = \sum_{r}^{d} f(a,b,c,d,r)$, where f is a well behaved function. Furthermore, we can write this result as

(3.4.2)
$$I_{abcd} = \sum_{r=0}^{d} \exp\{\log[f(a,b,c,d,r)]\}.$$

Note that f must be positive.

The logarithm $\log(f)$ is given by

(3.4.3)
$$\log(f) = -\frac{1}{2}\log(2) - 2\log(\pi)$$
$$+ \frac{1}{2}(\log(c!) + \log(d!) - \log(a!) - \log(b!))$$
$$- \log((d-r)!) - \log((c-d+r)!) - \log(r!)$$
$$+ \log\left(\Gamma\left(\frac{a+b-c+d+1}{2} - r\right)\right)$$
$$+ \log\left(\Gamma\left(\frac{a-b+c-d+1}{2} + r\right)\right)$$
$$+ \log\left(\Gamma\left(\frac{-a+b+c-d+1}{2} + r\right)\right).$$

Notice that due to the presence of the gamma functions, the previous expression could require the evaluation of a logarithm of a negative quantity. For this reason, we calculate instead $\log(|\Gamma(n)|)$, and compute the associated phase separately. This phase is introduced in the final expression after the exponentiation. Thus, the final expression of the integral taking into account the possible negative values of gamma functions reads

(3.4.4)
$$I_{abcd} = \sum_{r=0}^{d} p \exp\{\log[f(a,b,c,d,r)]\},$$

where p is the phase, given by $p = \prod_{n=1}^{3} p_n$, with p_n being the phase generated by each gamma function.

The logarithm of the gamma functions and the associated phase are calculated as

(3.4.5)
$$\left. \begin{array}{l} \log\left(\Gamma\left(n + \frac{1}{2}\right)\right) = \frac{1}{2}\log(\pi) + \log((2n)!) - n\log(2) - \log((n)!) \ , \ p = 1 \\ \log\left(\left|\Gamma\left(\frac{1}{2} - n\right)\right|\right) = \frac{1}{2}\log(\pi) + 2n\log(2) + \log((n)!) - \log((2n)!) \ , \ p = (-1)^n \end{array} \right\}, n \geq 0.$$

The logarithm of a factorial is calculated as:

$$\log(N!) = \sum_{n=1}^{N} \log(n).$$

(3.4.6)

3.5 A benchmark for two particle system

In general, it is not possible to solve exactly the energy spectrum. In our case, to determine the energy spectrum we have to diagonalize the Hamiltonian in a large Hilbert space by using sophisticated numerical techniques. However the case of two particles has been analytically solved in the literature [27].

3.5.1 Theoretical spectrum for two particles

For two fermions with opposite spin, $M = 0$, the energies of the relative motion are obtained by solving the transcendental equation [27]

$$\frac{\Gamma(-E_r/2 + 3/4)}{\Gamma(-E_r/2 + 1/4)} = -\frac{g}{2^{3/2}},$$

(3.5.1)

where Γ are gamma functions, E_r is the energy of the relative system and g is the interaction strength.

In addition, the center of mass is governed by an harmonic oscillator Hamiltonian Eq. (2.1.8), and its energy is given by Eq. (2.1.3). Then, the energy of a two-body state is the sum of its relative and center of mass energies. Therefore, each relative state has their corresponding center of mass excitations.

These analytical results are used as a benchmark of our numerical calculations and allow us to critically analyze the dependence of the numerical results on the size of the Fock subspace used in the diagonalization. As g increases one needs a larger subspace.

3.5.2 Comparison of analytical and numerical results

In Fig. 3.1 we report as a function of g the low energy part of the two-particle energy spectrum calculated by exact diagonalization (solid green line) and the spectrum obtained by solving Eq. (3.5.1). Notice that this equation provides the energy of the relative motion to which we add the energy of the center of mass: E_{CM}. For the ground state, $E_{CM} = 1/2$. The diagonalization has been performed using 100 single-particle modes that translates when the energy restriction is taken into account in a dimension of 5050 of the matrix to be diagonalized.

We explore both, the attractive and the repulsive interaction regimes. In general, for small values of $|g|$, both attractive and repulsive, the agreement between both types of calculations is
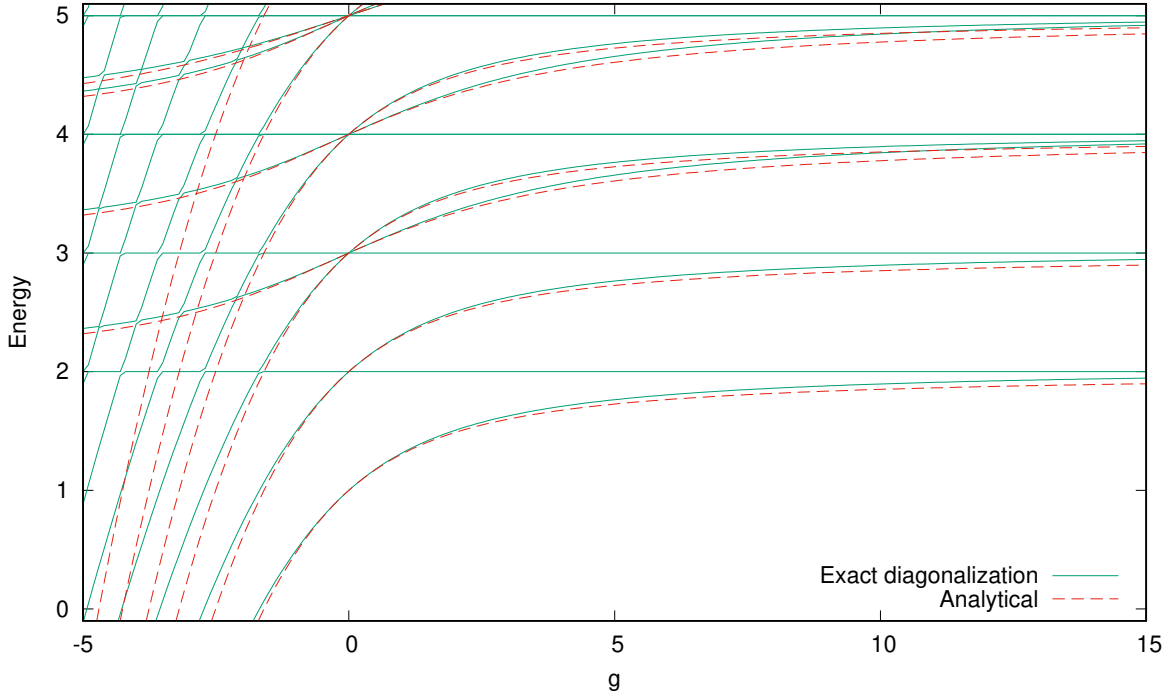
Figure 3.1: Energy spectrum of the two-particle system. The calculations are performed using 100 single-particle modes (solid green line). The analytical spectrum (dashed red line) is obtained with Eq. (3.5.1) for the energy of the relative system and adding after the possible energies of the center of mass.

very good. Apparently, the quality of the results deteriorates faster for attractive interaction. The calculations discussed in this thesis will consider mainly repulsive interactions which will be explored up to the strength interaction limit which is almost reached for the highest values of g considered, $g = 15$.

In the plot, we also include the horizontal lines which are energies of states not affected by the interaction. The first one corresponds to state with $S = 1$ and $M = 1$ which wave function can be decomposed as an antisymmetric wave function in coordinate space built with the single-particle states: $n = 0, 1$ times the triplet spin state with $M = 1$. The energy of this state, $E = 2$, does not depend on g, and it will be described in detail in a later chapter.

To complete the study of the accuracy of our calculations we investigate the convergence of the energy of the ground state and first excited state of the two particle system as a function of the number of harmonic oscillator modes used (N_M). Note that for $N = 2$, the energy constraint for the construction of the two-body basis is given by the maximum energy $E_{max} = 1/2 + (N_M - 1/2) = N_M$.

To this end, in Fig. 3.2 we report the difference between the ground state energy obtained by the
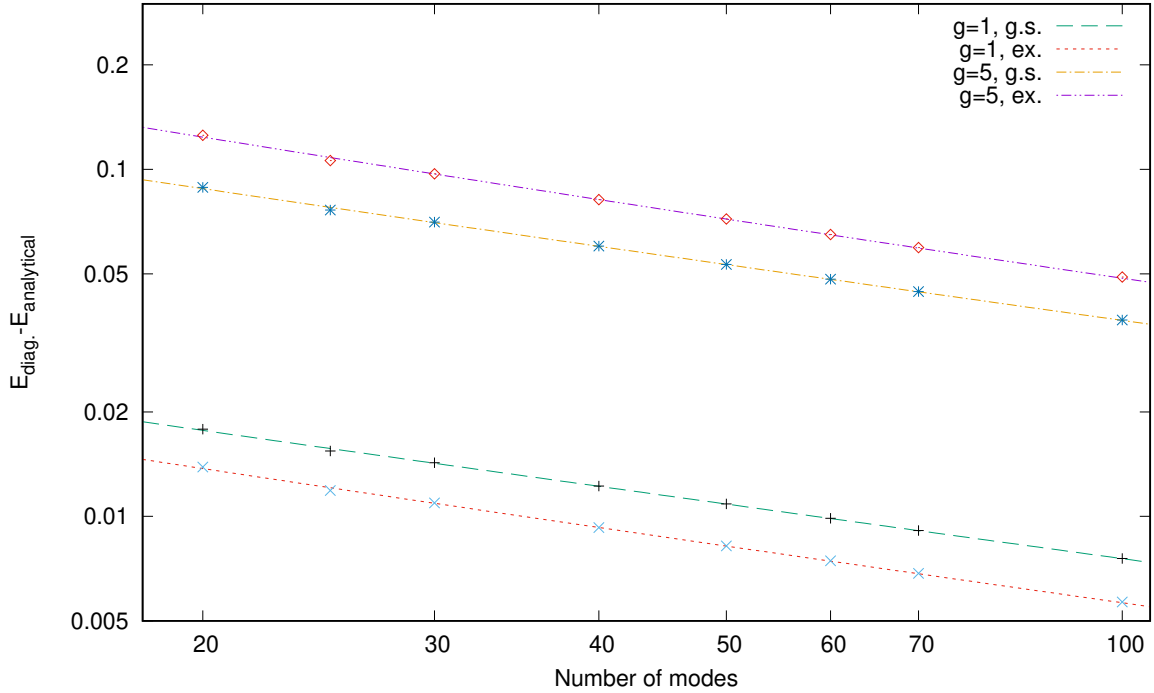
Figure 3.2: Differences between the numerical results and the exact ones as a function of the number of single particle modes, for two values of the interaction strength, $g = 1$ and $g = 5$, for the ground and first excited state. The lines are fits of the type $C_1/N_M^{1/2} + C_2/N_M$ to the calculated points. Notice that both axis are in a logarithmic scale.

diagonalization procedure and the analytical ones, for two values of the interaction strength. The figure also reports the difference of the first excited state. For $N = 2$, it is possible to establish the dependence of the dimension of the Hilbert space on N_M, which is given by $N_M(N_M + 1)/2$. As expected, the difference between the calculated and the expected value decreases with the number of modes. Following Ref. [31], we fit functions of the type $C_1/N_M^{1/2} + C_2/N_M$ with excellent results. In addition, for large values of N_M, the convergence of the energy goes as $1/N_M^{1/2}$. This dependence indicates a slow convergence of the numerical results by increasing the number of single-particle modes. As expected, the differences are larger for the larger strength, but in both cases the differences are very small. In all cases the difference is positive, indicating that the numerical results are upperbounds to the exact ones.

In this chapter we will discuss and analyze different observables characterizing the ground state of the system. This analysis will be done for several particle configurations and spin projections, devoting special attention to the two-particle system, as it is the only one with analytical solution.

In order to obtain the ground state of the system we will first calculate and diagonalize the Hamiltonian. The lowest eigenvalue is the energy of the ground state which is described by the corresponding eigenvector.

Notice that, we are working on a Fock space, and the eigenvectors are expressed in terms of the Fock basis. Therefore the ground state is written as

$$(4.0.1) \qquad |\Psi\rangle = \sum_n C_n |\psi_n\rangle ,$$

where $|\psi_n\rangle$ is a vector of the many-body basis of the Fock space.

4.1 Energy and virial theorem

The energy of the ground-state as a function of the interaction strength g for several number of particles and spin configurations is shown in Fig. 4.1. One can observe that in all cases, the ground-state energy becomes more repulsive when g increases and tends to saturate when $g \to \infty$. More precisely, for the $N = 2$, $M = 0$, the energy evolves from $E = 1$ at $g = 0$, the particles occupy the single particle states : $\{0\uparrow, 0\downarrow\}$, to $E = 2$ in the limit $g \to \infty$, in this case the particles occupy the states $\{0\uparrow, 1\downarrow\}$. For $N = 3$, $M = 1/2$ the energy goes from $E = 5/2$, the particles are in $\{0\uparrow, 0\downarrow, 1\uparrow\}$ states, to the $E = 9/2$ for $g \to \infty$, this means the single-particle states: $\{0\uparrow, 1\downarrow, 2\uparrow\}$. The same argument lead to the conclusion that for $N = 4$, $M = 0$ the energy goes from $E = 4$ at
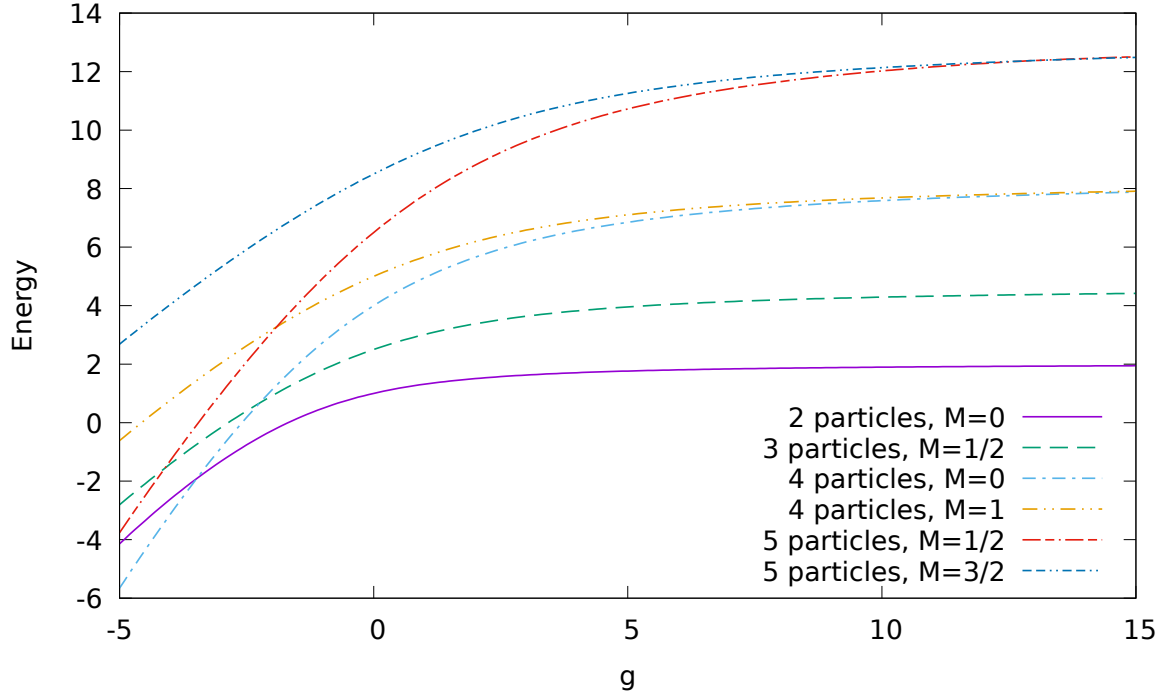
Figure 4.1: Ground state energy as a function of the interaction strength for different number of particles and spin configurations. The calculations have been performed using 100, 50, 40 and 30 single-particle modes to construct the many-body basis for N=2,3,4 and 5 particles respectively.

$g = 0$ to $E = 8$ at $g \to \infty$ while for $N = 4$, $M = 1$ the energy goes from $E = 5$ to $E = 8$. Notice that in the limit $g \to \infty$ the energy depends only on the number of particles and it is the same for the different spin projections. The values of the energy at $g \to \infty$ are predicted by the Eq. (2.2.4). On the other hand, in the case of an attractive interaction, the binding energy increases as the interaction becomes more attractive. In this case there are crosses between the energies belonging to different number of particles as the systems with more particles can accumulate more attraction.

After this general view of the evolution of the ground-state energy of different systems, we are going to analyse in more detail the two-particle system with $M = 0$, which energy as a function of g is plotted in Fig. 4.1. In the non-interacting case, the wave function can be factorized

$$(4.1.1) \qquad \qquad \Psi_{g=0}(1, 2) = \Phi_0(x_1)\Phi_0(x_2)\chi(S = 0, M = 0),$$

as a symmetric function in space with both particles in the same single-particle state and the two-body spin function corresponding to a singlet state which is antisymmetric: then the total wave function is antisymmetric and its energy is $E = 1$. In the limit of a very strong interaction,
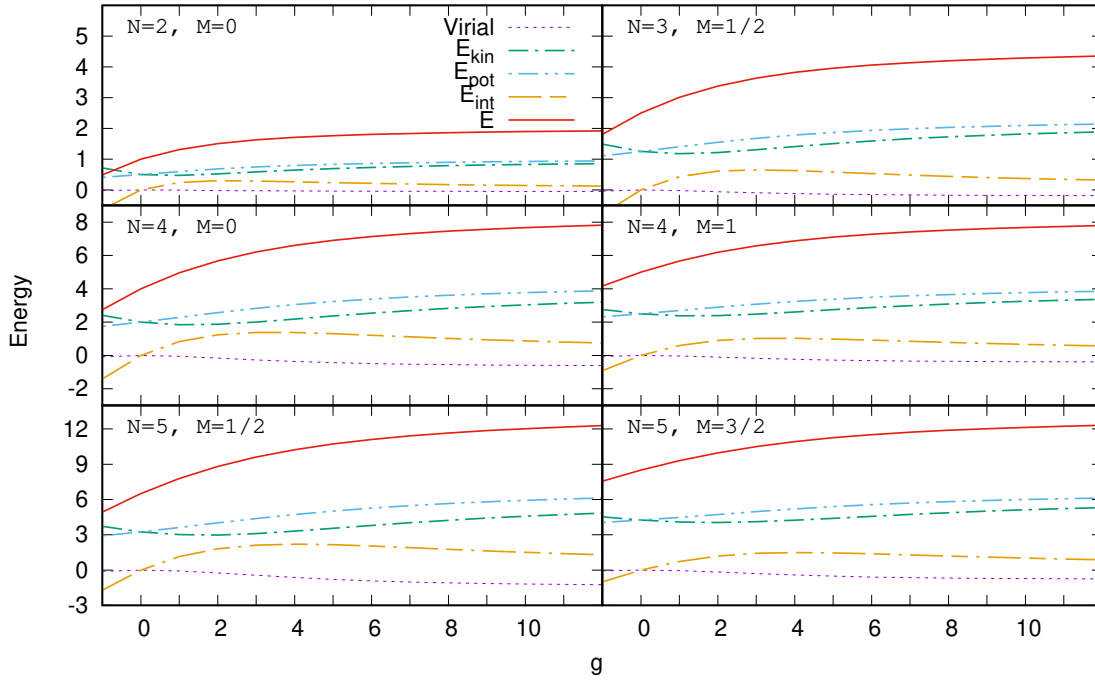
Figure 4.2: Different energy contributions to the total ground-state energy, as a function of the interaction strength for different number of particles and total third-spin component. The total energy and the fulfilment of the virial theorem is also shown (Eq. (4.1.3)). The legend is common to all graphics.

the wave function can be factorized as [32]

$$(4.1.2) \qquad \Psi_{g=\infty}(1,2) = \frac{1}{\sqrt{2}}|\Phi_0(x_1)\Phi_1(x_2) - \Phi_1(x_1)\Phi_0(x_2)|\chi(S=0, M=0)$$

i.e., the absolute value of the determinant built with the ground and first excited single-particle states of the confining harmonic oscillator times the singlet two-particle spin function. Notice that the presence of the absolute value ensures that the spatial part of the wave function is symmetric. Notice also that this wave function does not allow two particles to be at the same position and therefore the two particles do not feel the interaction. The final energy of this wave function is the sum of the single-particle energies, $E = 1/2 + 3/2 = 2$.

It is also interesting to study the decomposition of the energy in different pieces: kinetic, harmonic oscillator potential energy and interaction energy, which are constrained by the virial relation:

$$(4.1.3) \qquad 2\langle T\rangle - 2\langle V_{\text{ho}}\rangle + \langle V_{\text{int}}\rangle = 0\,.$$

The fulfilment of this relation reinforces the accuracy of the calculations. The derivation of the virial relation can be found in Appendix B.

In Fig. 4.2, we report as a function of the interaction strength the different contributions to the ground-state energy, for different number of particles and total third-spin component. The total energy is also reported. In general, for all cases considered, the behavior of the different contributions as a function of the interaction strength is rather similar. For a repulsive interaction, the total energy increases. In the repulsive interaction range, both the kinetic energy and the oscillator potential are similar and tend to the same value in the limit of infinite interaction. Also, the oscillator potential energy is greater than the kinetic energy in this range. The interaction energy starts from zero in the non-interacting case, has a maximum and goes to zero as the interaction strength tends to infinity.

In general the virial theorem is well fulfilled, although it deteriorates a little when the interaction strength is increased. In any case, the fulfilment of the virial theorem provides an additional test of the accuracy of the results. The behavior of the different contributions to the energy can be explained by taking into account the virial theorem and knowing the non-interacting and infinite-interacting limits. In the non-interacting case, the kinetic energy is equal to the oscillator potential energy. In the infinite interacting limit,the wave function is given by Eq. (4.1.2), that prevents to have two particles at the same position, therefore, the interaction energy is zero. As a consequence, the kinetic and the harmonic oscillator energies are also equal and fulfill the virial relation. For intermediate interactions, the interaction energy is positive, and the kinetic energy is lower than the oscillator potential energy in agreement with the virial theorem. The continuity of the interacting energy between zero and infinite interaction allows us to predict the existence of a maximum of the interaction energy as a function of g. On the other hand, when the interaction is attractive, the interaction energy takes negative values, increasing the binding energy as the interaction becomes more attractive. At the same time, the kinetic energy grows and the harmonic potential energy decreases, as a consequence of the decrease of the size of the system.

4.2 One body density matrix

Another interesting quantity that provides a lot of insight on the structure of the system is the one-body density matrix (OBDM), from which one can obtain the natural orbits, the momentum distribution and the density profile of the system. In second quantization, the matrix elements of the OBDM associated to $|\Psi\rangle$ are defined as,

$$(4.2.1) \qquad \rho_{ij} = \langle \Psi | a_j^\dagger a_i | \Psi \rangle = \sum_{n,m} C_n^* C_m \langle \psi_n | a_j^\dagger a_i | \psi_m \rangle \,.$$

4.2.1 Density profile

The first observable to be calculated is the density profile of the ground state of the system, that provides information on how the particles are spatially distributed in the trap.
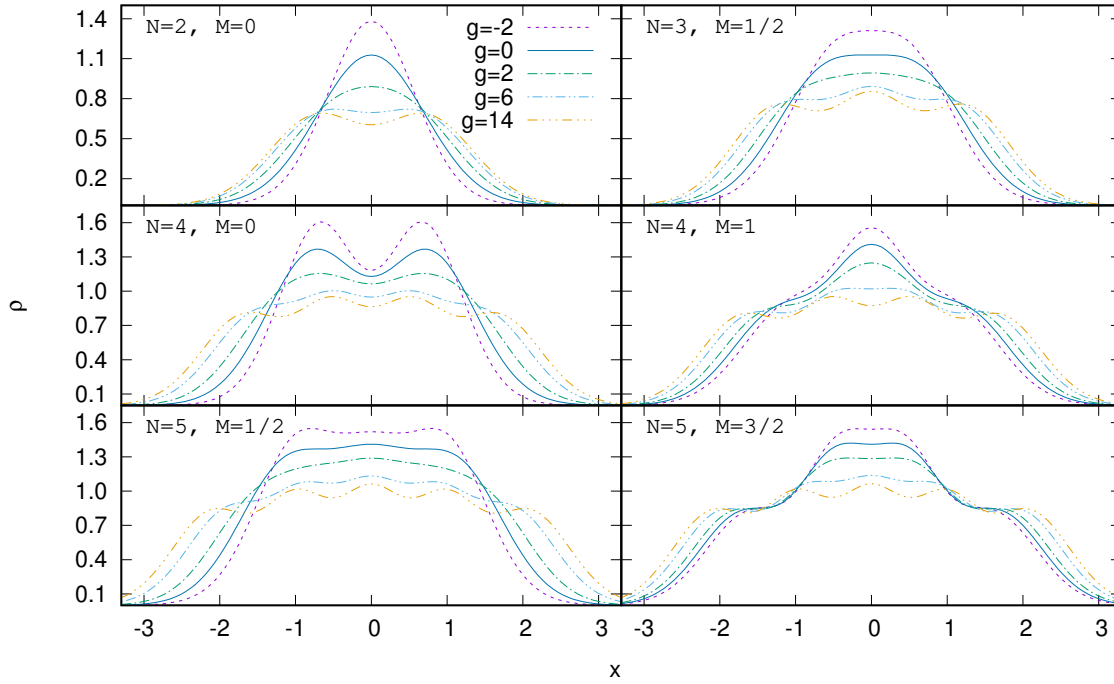
Figure 4.3: Density profiles of the ground state for different number of particles and spin projections. The density profiles are shown for various values of the interaction strength. The legend is common to all panels.

The density profile in terms of the matrix elements of the OBDM is given by:

$$\rho(x) = \sum_{i,j} \Phi_i^*(x)\rho_{ij}\Phi_j(x), \tag{4.2.2}$$

where $\Phi_n(x)$ are the single-particle wave functions used to construct the many body basis.

In Fig. 4.3 we report the density profile of the ground state of the system for different number of particles and spin configurations and for several several values of the strength interaction. As expected the density profiles at $g = 0$ for the different systems fully agree with the analytical expressions given in Eq. (2.2.2). For large values of g , $g = 14$ in the figure, the density profiles are very close to the ones predicted in Eq. (2.2.5). The small differences are due to the finite value of g and also to the finite size of the Hilbert space where we are diagonalizing the Hamiltonian. In any case, both for the energy and the spatial distribution of the particles, $g = 14$ can be considered a strongly interacting regime. Notice, that for the same number of particles and different spin configurations the density profiles are rather different, when g is small. However, for $g \to \infty$ the profile for a given number of particles does not depend on the spin projection. In the strong interacting limit, the density profile shows as many peaks as the number of particles, i.e. the particles try to be distributed equidistantly to minimize the repulsion. As it has been previously

commented, in most of the cases, when $g \to \infty$ the wave function minimizes the interaction energy by avoiding two particles to be in the same place. The size of the system also increases with the interaction strength.

4.2.2 Natural orbits

The diagonalization of the density matrix provides the natural orbits and its eigenvalues which can be interpreted as the occupation number of the natural orbits. The sum of the eigenvalues of the natural orbits are normalized to the total number of particles.

In the non-interacting case, the ground state of a N-particle system, which corresponds to a Slater determinant build with N single-particle harmonic oscillator functions with their spin projection, produces a OBDM with N-natural orbits with eigenvalue 1 and the all others with eigenvalue zero. In these cases the natural orbits can be identify with the single-particle wave functions used in the construction of the Slater determinant. When turning on the interaction, one gets a set of N-natural orbits with eigenvalues smaller than 1 and additional natural orbits with eigenvalues significantly smaller. The natural orbits are expressed as linear combinations of the harmonic oscillator single-particle basis and the Slater determinant built with the N natural orbits with the highest eigenvalues define the mean-field wave function with largest overlap with the ground state. The fact that the OBDM has eigenvalues smaller than 1 points out the existence of correlations beyond the mean-field in the ground-state of the system which translate in the impossibility to express the ground-state wave function as a single Slater determinant.

The eigenvalues associated to the natural orbits can be interpreted as the occupation numbers of the single-particle states defined by the natural orbits. Notice also that a given natural orbit does not mix single particle states with different parity or spin projection.

In Fig. 4.4 we report the dependence of the highest ten eigenvalues of the one-body density matrix as a function of the interaction strength for the ground-state of systems with different number of particles and spin projections. At $g = 0$ we have N, being N the number of particles, eigenvalues equal to unity, and the rest equal to zero. These eigenvalues correspond to the natural orbits which can be identify with the single-particle wave functions used to build the Slater determinant associated to one of the many-body basis states. When the interaction increases, the highest eigenvalues decrease indicating the presence of correlations in the system. Then as the eigenvalues are normalized to N, the smaller eigenvalues start to increase. As mentioned before, this indicates the impossibility to describe the wave function with only one Slater determinant.

Another interesting fact is that for $N = 2$ and $M = 0$ the eiganvalues appear with degeneration 2 independently of the value of g. One corresponds to spin up and the other to spin down that
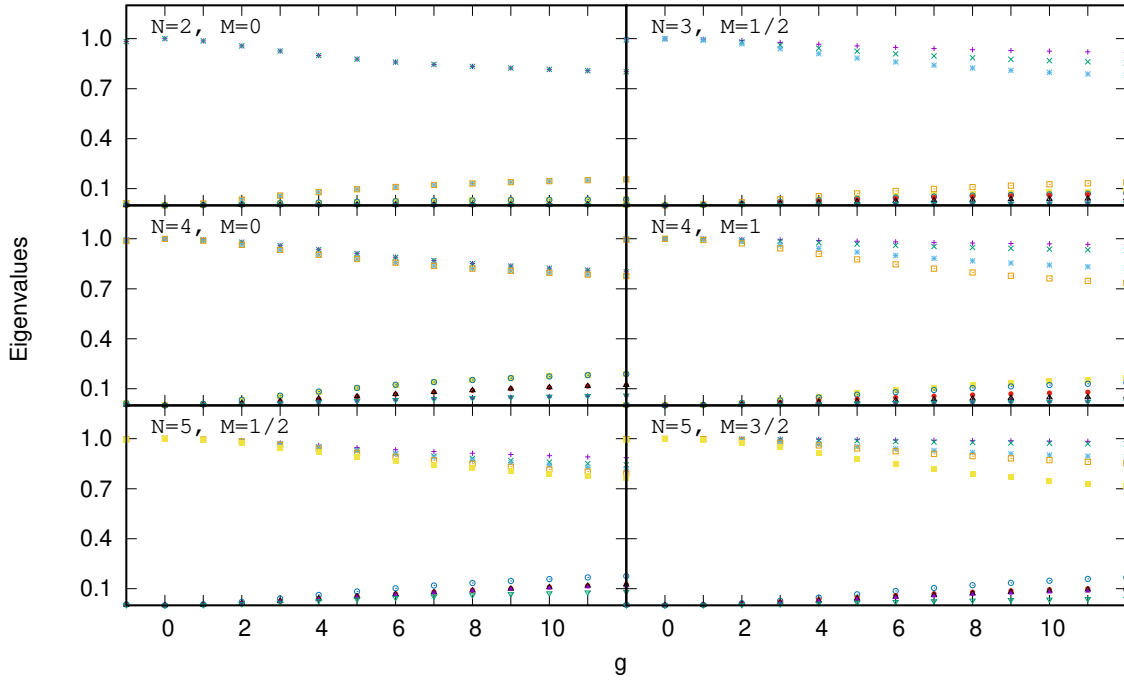
Figure 4.4: The largest ten eigenvalues of the OBDM of the ground state of systems with different number of particles and spin configurations as a function of the interaction strength.

have identical space distribution in the system. Actually the natural orbits do not mix different single-particle spin projections. This fact is also true for the system with $N = 4$ and $M = 0$. In this case we have at $g = 0$ four natural orbits, two corresponding to the single-particle state $n = 0$, both with spin up and spin down and the other to $n = 1$ also with both spin projections, all with eigenvalue equal to unity. Then when the interaction increases, the natural orbits mix higher excited harmonic oscillator states but do not mix the spin projection. The natural orbits are independent of the spin projection and the eigenvalues separate in two groups each one with degeneracy two. They have not only the same eigenvalue but also the same spatial structure. Instead, for $N = 3$ and $M = 1/2$ the natural orbits of each spin projection are different.

The explanation of these facts is because the OBDM is constructed in boxes of well defined third spin component :

$$(4.2.3) \qquad \begin{pmatrix} \rho_{\uparrow\uparrow} & \rho_{\downarrow\uparrow} \\ \rho_{\uparrow\downarrow} & \rho_{\downarrow\downarrow} \end{pmatrix} = \sum_{n,m} C_n^* C_m \langle \psi_n | \begin{pmatrix} a_\uparrow^\dagger a_\uparrow & a_\downarrow^\dagger a_\uparrow \\ a_\uparrow^\dagger a_\downarrow & a_\downarrow^\dagger a_\downarrow \end{pmatrix} | \psi_m \rangle \, .$$

However, the cross terms are zero and only the diagonal terms contribute. Therefore the matrix separates in two pieces one with spin up and the other with spin down. If the system is symmetric in the third spin component, both subspaces are equal and the eigenvalues and spatial eigenfunctions of each subspace are also equal.
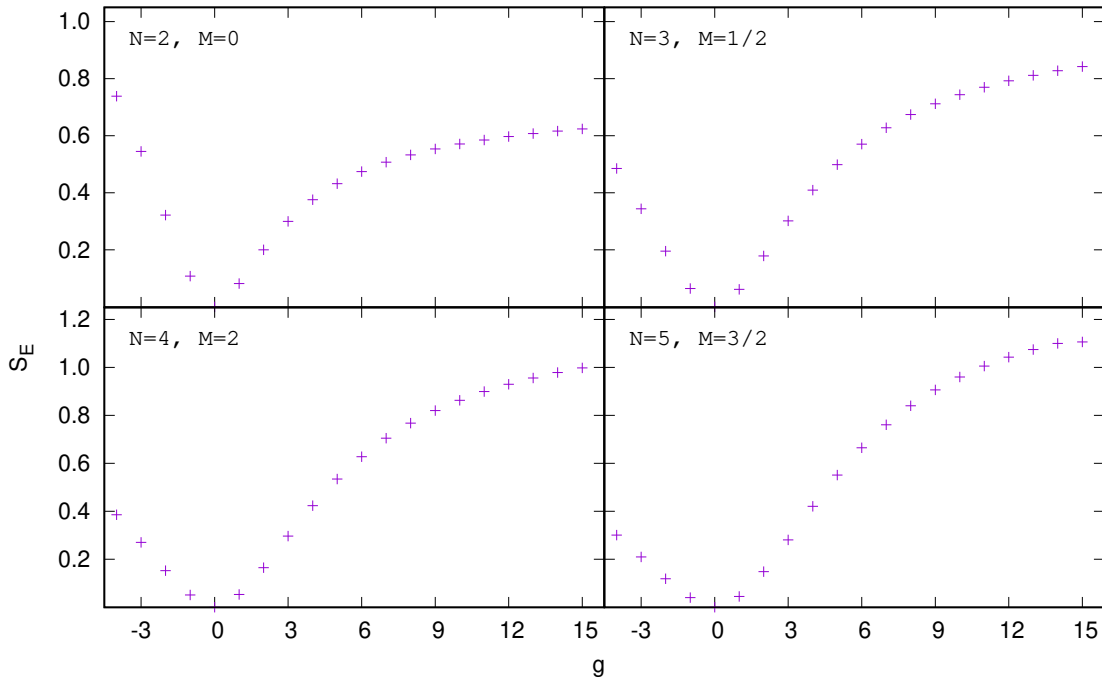
Figure 4.5: Entanglement entropy between the spin-up and the spin-down particles of a system with $N-1$ spin up particles and 1 spin-down particle as a function of the interaction strength, for several number of particles.

4.3   Entanglement

The concept of entanglement is a useful tool to explore the existence of quantum correlations in a system. A practical way to quantify the entanglement is by means of the entanglement entropy [33–35]. Our purpose is to study the entanglement between the spin-up and the spin-down particles in a few-body system. In particular, we only consider systems with one spin-down particle. This type of configurations can be view as a system with one spin impurity [36]. The objective is to calculate the entanglement entropy between the part of the system of particles with spin-up and the spin-down impurity.

4.3.1   Entanglement entropy

The first step towards the calculation of the entanglement entropy is to construct the reduced density matrix which is obtained by performing the trace of the density matrix of the ground state over the part of the system for which we want to measure the entanglement entropy with the rest of the system. In our case, the trace should be taken over the particle with spin down.

The density matrix of the ground state is :

(4.3.1)
$$\hat{\rho} = |\Psi_0\rangle \langle \Psi_0|$$

where the ground state can be expressed in terms of the many-body basis states of the N particle states,

(4.3.2)
$$|\Psi_0\rangle = \sum_n C_n |\psi_n\rangle.$$

To construct the reduce density matrix, we have to perform the trace of $\hat{\rho}$ over the particle with spin-down. To this end, we consider the many-body basis of the system of $N-1$ spin-up particles, which we denote by $|\phi_i\rangle$, $i = 1, 2, ...$ Then we construct the many-body basis of the system with $N-1$ particles of spin up and one particle with spin down (which has been used in Eq. (4.3.1)) by adding a particle with spin down in all possible single-particle harmonic oscillator states to each of the states $|\phi_i\rangle$. Thus the basis of the N particles can be written as $a_{i,\downarrow}^\dagger |\phi_j\rangle$; $i = 1, 2, ..., j = 1, 2, ...,$ where the index i runs over the harmonic oscillator states and the index j over all the basis-states of the $N-1$ particles of spin up.

Now, we can evaluate the matrix elements of the reduce the density matrix, which is an operator in the Hilbert space of the remaining $N-1$ particles:

(4.3.3)
$$\rho_r(\phi_i, \phi_j) = \langle \phi_i | \hat{\rho}_r | \phi_j \rangle = \sum_k \langle \phi_i | a_{k,\downarrow} |\Psi_0\rangle \langle \Psi_0| a_{k,\downarrow}^\dagger |\phi_j\rangle$$
$$= \sum_{n,m,k} C_n C_m^* \langle \phi_i | a_{k,\downarrow} |\psi_n\rangle \langle \psi_m| a_{k,\downarrow}^\dagger |\phi_j\rangle.$$

where $|\phi_i\rangle$, $i = 1, 2, ...$ are the $N-1$ spin-up particle basis and $a_{i,\downarrow}^\dagger (a_{i,\downarrow})$ are the creation (annihilation) harmonic oscillator operators.

Once we have the matrix representation of the reduce density matrix we procede to its diagonalization and obtain its eigenvalues $\rho_{r,i}$ which will be use to evaluate the entanglement entropy by using the Shannon prescription:

(4.3.4)
$$S_E = -\sum_i \rho_{r,i} \log[\rho_{r,i}].$$

In Fig. 4.5 we report the entanglement entropy between the spin-down particle and the spin-up particles for systems with different number of particles and spin configurations. Notice that in all cases there is only one spin-down particle. For all systems, the entanglement entropy is zero in the non-interacting case and the entanglement entropy grows when the interaction strength increases, both in the repulsive and and attractive regimes. In the infinite interacting limit, the entanglement entropy tends to saturate to a finite value, different for each number of particles which increases with N.

To complete the study of the structure of the few-body fermions systems, in this chapter we discuss the low energy excitation spectrum which will be useful to understand the dynamics and the response of the system to an external perturbation.

5.1 Energy spectrum

Once the Hamiltoninan for a given number of particles (N) and total third spin component (M) has been diagonalized, we have access to the spectrum and the structure of the eigenstates. We pay particular attention to the dependence on the interaction strength of the low energy part of the spectrum, which is shown in Fig. 5.1 for several number of particles and spin configurations.

The first observation is the existence of states which are not affected by the interaction and therefore appear as horizontal lines in the plots. These states correspond to antisymmetric wave functions in space and give zero probability of having two particles in the same position. Therefore the particles described by this wave function do not feel the contact interaction.

Another general observation is the existence of excitations with a constant energy shift independent on the interaction strength which are associated to excitations of the center of mass of the system of top of a given state. Notice that the interaction which is translational invariant does not affect the center of mass motion.

An interesting feature is that the energy of all states saturate when the interaction strength tends to infinity. Actually, some states merge to the same energy when $g \to \infty$ increasing the degeneracy of the energy levels in this limit.
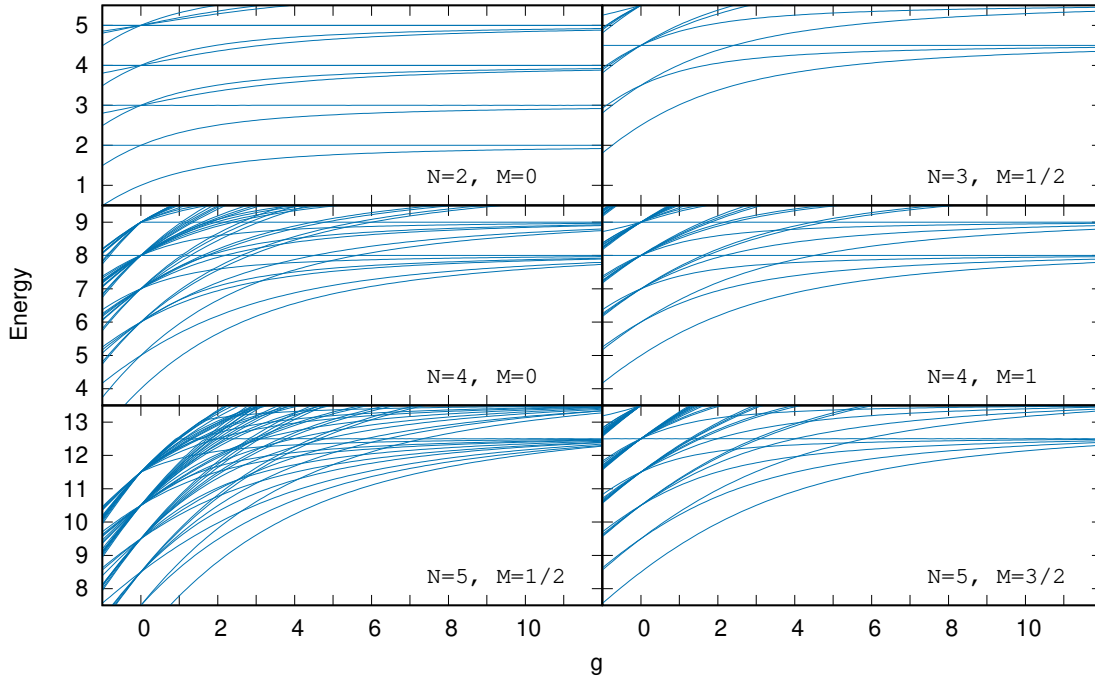
Figure 5.1: Low spectrum for several number of particle and spin configurations. The 20 lowest energies obtained have been represented. Notice that in these spectra have been subtracted from the energy of the ground state in the case without interaction.

Let us analyze more carefully the case $N = 2$ and $M = 0$. As explained in the previous chapter, the non-interacting ground state corresponds to

$$\Psi(1,2) = \Phi_0(x_1)\Phi_0(x_2)\chi(S = 0, M = 0), \tag{5.1.1}$$

with energy $E = 1$. The two first excited levels have the same energy, $E = 2$ at $g = 0$, one corresponds to a state

$$\Psi(1,2) = \frac{1}{\sqrt{2}}(\Phi_0(x_1)\Phi_1(x_2) - \Phi_1(x_1)\Phi_0(x_2))\chi(S = 1, M = 0), \tag{5.1.2}$$

which is a product of antisymmetric in coordinate space and a symmetric one in spin. This state is not affected by the interaction and its energy is independent of g. The energy of this state merges with the ground state energy when $g \to \infty$. As the Hamiltonian commutes with the spin, this state will be degenerated with states having the same spatial wave function and the spin functions corresponding to $S = 1$ but $M = 0, \pm 1$, which can not be distinguished in the plot.

The other excited state at $g = 0$ corresponds to

$$\Psi(1,2) = \frac{1}{\sqrt{2}}(\Phi_0(x_1)\Phi_1(x_2) + \Phi_1(x_1)\Phi_0(x_2))\chi(S = 0, M = 0), \tag{5.1.3}$$

which is symmetric in spatial coordinates and antisymmetric in spin. It can be shown that this state corresponds to the first excitation of the center of mass times the intrinsic wave function of the ground state described above. In the ground state, the center of mass is always in the ground state of H_{CM}. However in the state we are considering the center of mass occupies the first excited state of H_{CM}, this is true for all values of g and the energy of this state can be written as $E = E_{g.s.} + 1$ along all values of g. This state has degeneracy one.

This type of arguments explain the full spectrum for $N = 2$. It is worth to remember that our numerical procedure is constructed in the Fock space using single-particle wave functions, without the decomposing of the Hamiltonian in the center of mass and intrinsic parts. Therefore the exact localization of the center of mass excitations provides a test on the numerical accuracy of the calculations.

We continue our analysis by considering the case for $N = 3$ and $M = 1/2$. The ground state at $g = 0$ has an energy $E = 1/2 + 1/2 + 3/2 = 5/2$, which corresponds to a state that populates the single-particle harmonic-oscillator states: $\{0\uparrow, 0\downarrow, 1\uparrow\}$, that results in $M = 1/2$. Then when g increases, the state incorporates more complicated configurations, the energy increases monotonously and tends to $E_{g\to\infty} = 1/2 + 3/2 + 5/2 = 9/2$. The spin of the ground state is $S = 1/2$, which is the minimum compatible with the value of $M = 1/2$ and its parity is negative all along the values of g. At $g \to \infty$ the ground state merges with the state with $S = 3/2, M = 1/2$ which is a state built with a Slater determinant with the single-particle harmonic-oscillator states: $n = 0, 1, 2$ times the symmetric wave function of three spins $S = 3/2, M = 1/2$. The particles in this state do not feel a contact interaction and the energy of this state is independent of the interaction strength. Notice also the existence of two states at $g = 0$ with $M = 1/2$ built with the single-particle harmonic-oscillator states $\{0\uparrow, 0\downarrow, 2\uparrow\}$ and $\{0\uparrow, 1\downarrow, 1\uparrow\}$ which give origin at $g = 0$ to two states with total energy $E = 7/2$. One describes an excitation of the center of mass built on top of the ground state which evolves with g keeping always the same energy shift respect to the ground state, and the other state merges with the ground state when $g \to \infty$.

Next, we discuss the case $N = 4$ and $M = 0$. Of course, the number of levels increases with the number of particles and the number of levels is larger when the total spin projection, M is smaller. One immediately detects a state not affected by the interaction that corresponds to a state with $S = 2$, the maximum spin for $N = 4$ and $M = 0$. This state can be identified with a wave function that is the product of an antisymmetric wave function given by a Slater determinant built with the single-particle harmonic-oscillator states: $n = 0, 1, 2, 3$ and a symmetric spin function of four particles with $S = 2$ and $M = 0$. The total energy of this state, $E = 1/2 + 3/2 + 5/2 + 7/2 = 8$, is given by the sum of the first four single-particle energies of the harmonic-oscillator trapping potential. The ground state is a state with $S = 0$, i.e. the minimum total spin compatible with the

value of M. The energy of the state at $g = 0$, $E = 4$, corresponds to the occupation of the single particle levels: $\{0\uparrow, 0\downarrow, 1\uparrow, 1\downarrow\}$. The energy gets more repulsive as g increases and for $g \to \infty$ the energy merges with the energy $E = 8$ of the previously discussed state. The parity of the ground-state is positive. One can also identify the excitations of the center of mass characterized by a constant shift of the energy respect to the ground-state or on top of a given state. For instance, the first one corresponds to a center of mass excitation of one unit of energy of the Hamiltonian associated to the center of mass, H_{CM}. There are other levels which quantum numbers can be identified and many of them merge together when $g \to \infty$.

Similar comments apply to the case $N = 4, M = 1$. One can also identify the state not affected by the interaction, $S = 2, M = 1$, that has the same energy as the state $S = 2, M = 0$ of the previous panel. Here the ground state starts with $E = 9/2$ at $g = 0$ which corresponds to the Slater determinant built with the single-particle states: $\{0\uparrow, 0\downarrow, 1\uparrow, 2\uparrow\}$.

Finally let us discuss very briefly the case $N = 5, S = 1/2$. In this case, there are many levels below the first level not sensitive to the interaction strength, which has an energy $E = 1/2 + 3/2 + 5/2 + 7/2 + 9/2 = 25/2$ and $S = 5/2, M = 1/2$. The ground state, has $S = 1/2$, and positive parity. At $g = 0$ has an energy $E = 13/2$ and when $g \to \infty$ merges with the state non-sensitive to the interaction discussed above, which an energy $E = 25/2$

For the case with $M = 3/2$ there are much less levels. The ground state at $g = 0$ has more energy than the ground state for $M = 1/2$, basically due to the Pauli Principle. In fact, at $g = 0$ the ground-state is built with the single particle states $\{0\uparrow, 0\downarrow, 1\uparrow, 2\uparrow, 3\uparrow\}$, which gives an energy $E = 17/2$. However, when g increases the state merges with the state $S = 5/2, M = 3/2$ which is also degenerated with the sate $S = 5/2, M = 1/2$ discussed in the previous panel.

We have compared our results with the ones provided in Ref. [18] obtaining a good agreement in all cases considered. It is worth to point out that our results that can be considered variational are in general slightly below the results of Ref. [18].

As an important point, it is observed that at the limit of large interaction, we see that states begin to experience degeneration. We know that for the ground state this degeneration is expressed as $D = \frac{N!}{N_u! N_d!}$.

5.2 Spin determination

As the Hamiltonian does not depend on the spin, it commutes with the spin operators. In particular with S_- and S_+. Therefore, if we have a state with a total spin S and spin projection M

with energy E, due to the commutation relations of $S_{+(-)}$ with the Hamiltonian, it turns out that by applying the operators $S_{+(-)}$ to this state one obtains a state with the total spin projection increased (reduced) by 1, i.e, $M \pm 1$, with the same energy E. Therefore, for each eigen-energy state with a well defined spin, there will be $2S + 1$ states with the same energy. We can use this fact to determine the total spin of the states. The argument is as follows: Given N fermions, we start by the maximum possible spin projection, that will be the state with all spins up, with $M = N/2$. In this case, the wave function factorizes in a spatial antisymmetric wave function times a symmetric spin wave function. The total spin of this wave function coincides with the maximum value of the spin projection, $S = N/2$. Then if we apply $2S + 1$ times to this state the operator S_-, we will get all the states belonging to this spin multiplet, all having the same energy and all of them factorized as an antisymmetric wave function in space times a spin symmetric wave function. In the next step, we consider the Hamiltonian in the box with $M = S - 1$. Among the energies obtained in this box, one find the previous energy attributed to $S = N/2$, corresponding to the state with $M = N/2 - 1$.

One can inmediately assign the spin quantum number to the remaining states, which will be the minimum S compatible with the value of M, i.e. $S = N/2 - 1$. Notice that, one can have more than one state with this spin and one would need another quantum number to distinguish them. Next, we take the box of the Hamiltonian associated to the value of M, $M = N/2 - 2$. Here we will inmediately identify the energies obtained for the previous spin values and again the rest of states have an spin that will be the minimum compatible with the value of M. One can continue this process until the total spin projection has the positive lowest value (in the case of half-integer values) or zero value in case of integer M.

To illustrate this procedure, we consider the lowest energy states of the case $N = 4$ shown in Fig. 5.2 as a function of the interaction strength. The maximum possible spin projection is $N/2 = 2$. The wave function of this state can be factorized as a Slater determinant with the first four single particle states of the harmonic oscillator times a spin wave function with all spins up. The energy of this wave function, $E = 8$, is the sum of first four single-particle harmonic oscillator energies, $E = 1/2 + 3/2 + 5/2 + 7/2$. In addition, this state is not affected by the interaction and therefore appears as an horizontal line in figure. This energy level corresponds also to the energy of the different possible $2S + 1$ states corresponding to $S = 2$. In the next step we consider the box with $M = 1$. First we identify the previous energy and find out several eigenstates which can be all associated to $S = 1$ (red lines in the figure). Notice that all of them have different energies, but $S = 1$. For instance, at $g = 4$ we find three $S = 1$ levels with energies below $E = 8$. In the next step we diagonalize the subspace with $M = 0$ and detect the $M = 0$ states corresponding to $S = 2$ and to the $S = 1$ states detected before. The rest of levels have $S = 0$. At $g = 5$, we find also three $S = 0$ levels, all with different energy, and non degenerate. Notice that one of them corresponds to a
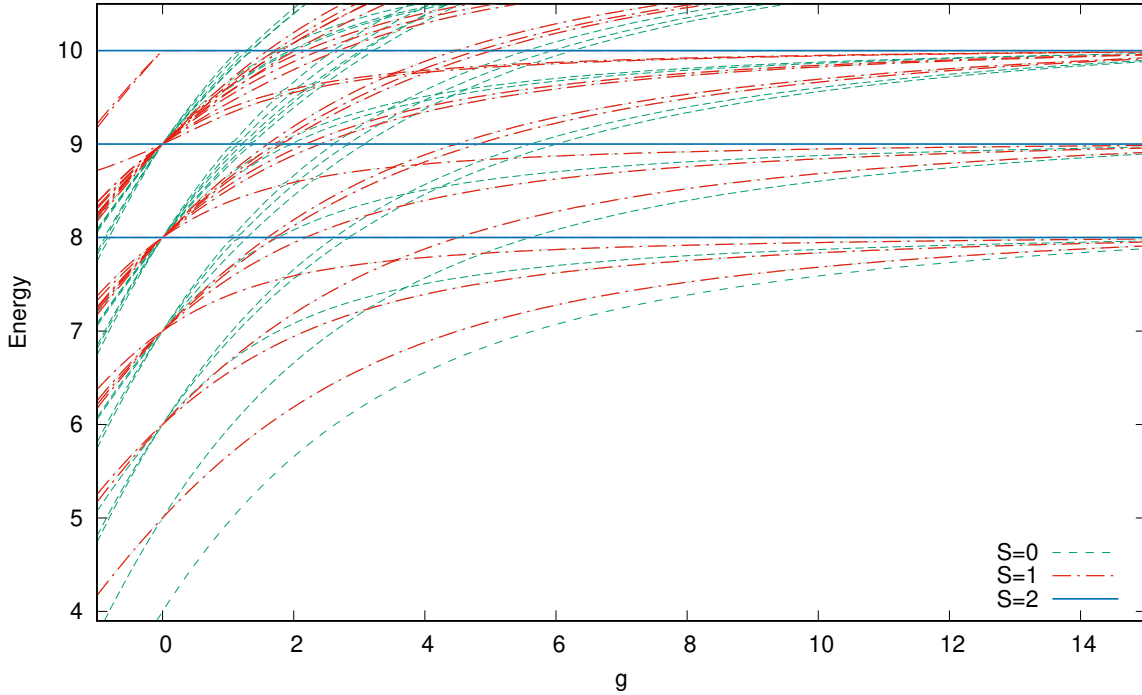
Figure 5.2: Spectrum for the case with four particles.

center of mass excitation that when $g \to \infty$ merges with other levels at $E = 9$. Using these type of arguments one can assign the spin to the energy levels even if the total wave function could be complicated and most of the times non-factorizable in a spin and a space part.

5.3   Parity of states

As the Hamiltonian commutes with parity, it is possible to use the parity as a quantum number to characterize the states. In particular, in the non-interacting case if the wave function is defined by a Slater determinant of single-particle wave functions, the parity associated to this state is given by $(-1)^{\mathcal{N}}$ where $\mathcal{N} = \sum n_i$, where n_i are the oscillator quantum numbers associated to the harmonic oscillator single-particle wave functions used to build the many-body state. Notice that the parity of a harmonic oscillator single-particle wave function $\Phi_n(x)$, $n = 0, 1, 2, 3...$, is given by the parity of n. At the same time the energy associated to this determinant is given by $E = \sum(n_i + 1/2) = \mathcal{N} + N/2$. One can argue that when the interaction is turned on very slowly, the parity of the evolved states does not change respect to the parity assigned in the non-interacting case. In this way, for $N = 2$, the parity of the ground state is positive for any value of g. The same is true for $N = 4$ with $M = 0$. However the ground state of $N = 3$ with $M = 1/2$ and $N = 4$ with $M = 1$ have negative parity.

To illustrate the assignation of parity to the excited states we consider the fist excited state for $N = 4$ and $M = 0$ to which one can assign negative parity (see Fig. 5.2). In fact, locking at the states at $g = 0$ one can built two Slater determinants one with the single-particle states $\{0 \downarrow 0 \uparrow 1 \downarrow 2 \uparrow\}$ and another with $\{0 \downarrow 0 \uparrow 1 \uparrow 2 \downarrow\}$ with the same energy $E = 5$. These two configurations give rise to two excited states one corresponding to a center of mass excitation of the ground state and the other to an intrinsic excitation. In both cases due to the presence of the state $1 \uparrow$ or $1 \downarrow$ the parity is negative and is kept negative independently of the value of g.

In general for excited states generated by excitations of the center of mass on top of the ground state, the parity of the excited state is given by the change in parity of the center of mass excitation. For instance, the first excitation of the center of mass shown for $N = 2$ and $N = 4$ with $M = 0$ have negative parity. Similar arguments allow to assign the parity number to all states.

6

DYNAMICAL EXCITATION

In previous chapters we have concentrated in the static properties of the fermionic system. In particular, we have analyzed the ground state and also the main features of the low-energy spectrum. In the present chapter we turn our attention to the dynamics of the fermionic mixtures in the harmonic trap. Simulating the dynamics of quantum many-body systems is important for current quantum technological applications where one could for instance design quantum systems to produce desired many-body states after a certain evolution [37–39]. A second relevant aspect is that the dynamics of the system reflects in many ways the internal structure. In this sense, one can devise dynamical evolution in order to unveil the spectral structure of the system [40]. This is the main goal of this chapter. To this aim we will consider two different perturbations to the ground state of the system which will be sensitive to the low-energy spectra presented before. The first will be a sudden change in the trap frequency. This perturbation excites both center of mass and relative modes of the system. In this case we will consider the dynamic structure function. The second one will be a sudden quench of the interaction strength. In this case, we will analyze how the internal structure influences the time evolution of the central density of the cloud.

6.1   Sudden change in the trap frequency: breathing mode

A well-known way of studying the internal structure of a quantum many-body system trapped in a harmonic oscillator is by exciting the so called breathing mode. In contrast with the Kohn (dipole) mode, where the cloud is initially displaced from the minimum of the potential [41], in our case we study the response of the system to a change in the trapping frequency. The main

tool we consider is the dynamic structure function associated to the mono-polar operator

$$(6.1.1) \qquad \hat{F} = \sum_j^N x_j^2 .$$

It is important to see that this perturbation preserves spin and parity, therefore, it will only connect the ground state of the system with other excited states with the same total spin and parity.

This operator can be separated in two pieces: a center of mass and an intrinsic one; $\hat{F} = NX_{\text{CM}}^2 + \frac{1}{N} \sum_{j<i} (x_i - x_j)^2$. The center of mass of the system is described by an harmonic oscillator Hamiltonian, and the wave functions associated to this part are the harmonic oscillator wave functions. Note that this perturbation can excite the center of mass or the intrinsic part, but not both at the same time.

6.1.1 Dynamic structure function

In order to know the response of the system to an external perturbation, one can compute the dynamic structure function. This function, normalized to the number of particles, is defined as

$$(6.1.2) \qquad S_F(E) = \frac{1}{N} \sum_{i>0} |\langle \Psi_i | \hat{F} | \Psi_0 \rangle|^2 \delta(E - (E_i - E_0)) ,$$

where $\hat{F}$ is the excitation operator associated to the external perturbation, is given by Eq. (6.1.1), $|\Psi_0\rangle$ is the ground state of the unperturbed system and $|\Psi_i\rangle$ are its excited states.

In second quantization formalism, the structure function reads,

$$(6.1.3) \qquad S_F(E) = \frac{1}{N} \sum_{i>0} \left| \sum_{n,m} C_{n,0} C_{m,i}^* \sum_{k,l} \langle k | x^2 | l \rangle \langle \psi_m | a_k^\dagger a_l | \psi_n \rangle \right|^2 \delta(E - (E_i - E_0)) ,$$

where $|k\rangle$ and $|l\rangle$ are single-particle states and $|\psi_n\rangle$ are the Fock states of our basis. For the center of mass system, the $\langle i_{\text{CM}} | X_{\text{CM}}^2 | j_{\text{CM}} \rangle$ are different from zero only when $i_{\text{CM}} = j_{\text{CM}}$ and $i_{\text{CM}} = j_{\text{CM}} \pm 2$. This implies that the center of mass only can be excited by two energy quanta.

In some limiting cases we know the analytic value of the dynamic structure function, these cases can be used to benchmark our numerical calculations [22]. For the non-interacting case, we expect a single peak in the dynamic structure function with an energy $E - E_0 = 2$. The intensity of this peak depends on the number of particles and the total spin projection. Likewise, in the infinite interaction limit, we also expect a single peak in the dynamical structure function with energy $E - E_0 = 2$. In addition, a peak with energy $E - E_0 = 2$ is expected for any value of the interaction strength, due to the center of mass excitation, with a constant intensity as a function of the interaction strength. In the range of repulsive interaction, we expect more peaks associated to states with the same spin and parity as the ground state. These correspond to intrinsic
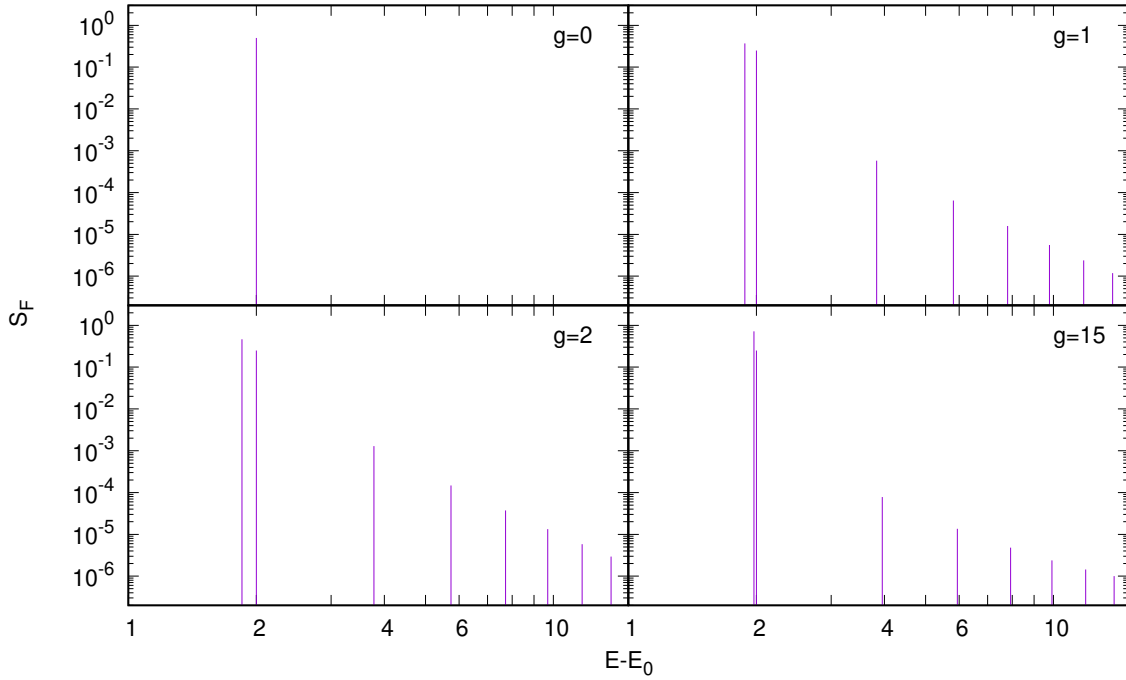
Figure 6.1: Dynamic structure function of a mono-polar excitation for the case of two particles. The total spin projection considered is zero. The different panels correspond to four different values of interaction strength. From the non-interacting case, $g = 0$ to a strongly interacting one $g = 15$.

excitations.

In Fig. 6.1 we present the dynamic structure function for the two-particle case for several values of the interaction strength, concretely for the non-interacting case and for values of the interaction strength $g = 1$, $g = 2$, and $g = 15$. As expected, for the non-interacting case we only have one peak at excitation energy $E - E_0 = 2$. For any interaction strength there is a peak at $E - E_0 = 2$ with the excitation energy associated to the center of mass excitation with an intensity independent of the interaction strength. The rest of the peaks observed are associated to intrinsic excitations. In addition, for large interaction strengths, we recover only one peak at $E - E_0 = 2$, and the rest of peaks vanish. The intensity of the excitations decreases for the states with more energy, and there is a dominant peak near the energy of the center of mass excitation. In the non-interacting case, the single peak has two contributions: the center of mass, and the dominant intrinsic peak. When we turn on the interaction, the dominant peak moves to a lower energy, but for large interaction, returns to the same energy than the center of mass excitation. This behaviour is named a reentrance behaviour [42], also observed in the energy spectrum for the two particles case. For secondary excitations, we can identify the correspondent states via the energy spectrum: all of them are excitations of the relative motion.
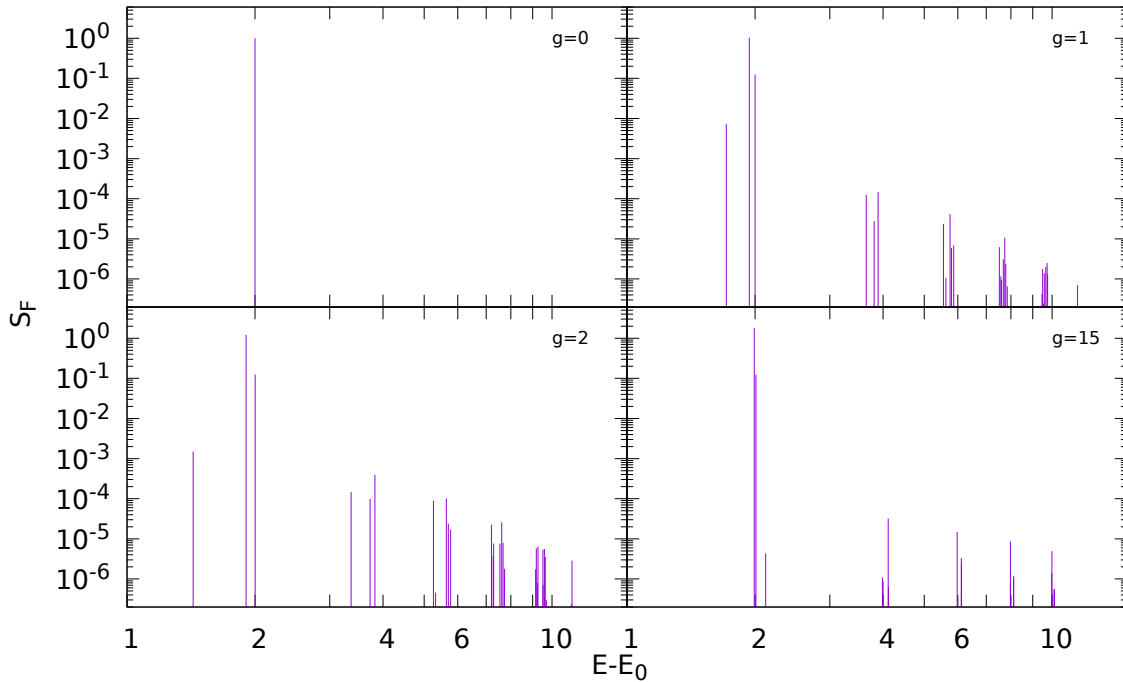
Figure 6.2: Dynamic structure function of a mono-polar excitation for the case of four particles. The total spin projection considered is zero. The different panels correspond to four different values of interaction strength. From the non-interacting case, $g = 0$ to a strongly interacting one $g = 15$.

In the case of $N = 2$ with $M = 0$, we can identify the center of mass and intrinsic excitations, because we know the analytic spectrum [27]. It is not the case for the rest of configurations. The $N = 4$ with $M = 0$ configuration is a good case to see the behaviour of the dynamic structure function of the breathing mode in a more complex case.

In Fig. 6.2 we report the dynamic structure function associated to the breathing mode for $N = 4$ with $M = 0$, for different values of the interaction strength, concretely, for the non-interacting case ($g = 0$), for $g = 1$, $g = 2$ and $g = 15$. As in the case of two particles, in the non-interacting case, there is only one peak with energy $E - E_0 = 2$. In the interacting case, there is a peak at energy $E - E_0 = 2$ with a constant intensity, which we identify with a center of mass excitation. All the peaks present can be associated to excitations of the ground state to states with the same spin and parity as the ground state. Using this information, we verify that the spin determination in Section 5.2 and the parity determination in Section 5.3 are in agreement with the results obtained here. Note that not all the states that verify these conditions (have the same spin and parity as the ground state) are excited. This is because the state has to be an intrinsic excitation or a center of mass excitation. In addition, in this case we also observe a dominant peak with a
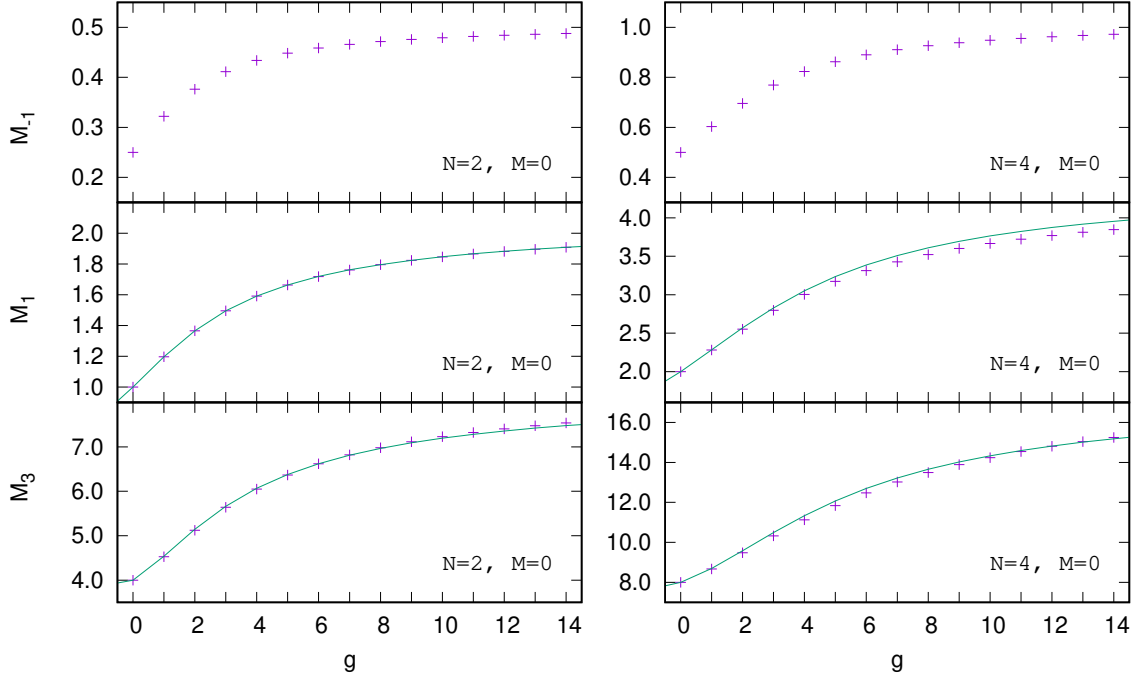
Figure 6.3: Values of the three energy momenta M_{-1}, M_1 and M_3 for the cases of two and four particles as a function of the interaction strength. The calculations are done using the explicit value of the dynamic structure function, Eq. (6.1.4) are represented by dots and the line is the value computed using the sum rules, Eq. (6.1.6).

reentrant behaviour. This is common to all the cases with different number of particles and total spin projection we have considered. Finally, we can see that in the limit of strong interaction, the intensity of all the peaks, except the dominant and the center of mass, decrease, tending to zero for the infinite interaction limit.

6.1.2 Sum rules

The energy moments of the dynamic structure function contain information of the response of the system to an excitation. They are defined as

$$(6.1.4) \qquad M_n = \int E^n S_F(E) dE \,,$$

and can be explicitly computed form the deifnition of $S_F(E)$ (Eq. (6.1.3)) by using the second quantization formalism as:

$$(6.1.5) \qquad M_n = \frac{1}{N} \sum_{i>0} \left| \sum_{n,m} C_{n,0} C_{m,i}^* \sum_{k,l} \langle k | x^2 | l \rangle \langle \psi_m | a_k^\dagger a_l | \psi_n \rangle \right|^2 (E_i - E_0)^n \,.$$

In the case that the dynamic structure function is known, the energy momenta can be computed directly using Eq. (6.1.5). But in general, the dynamic structure function is complicated and is
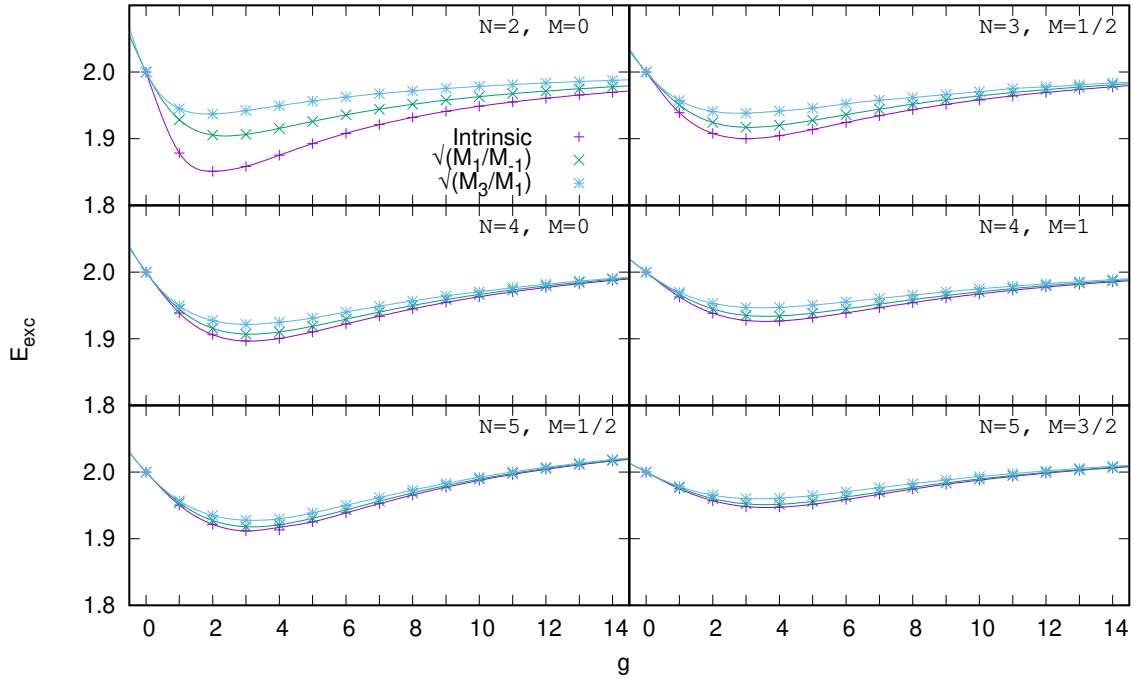
Figure 6.4: Ratios of the sum rules $\sqrt{M_1/M_{-1}}$ and $\sqrt{M_3/M_1}$ as a function of the interaction strength for several number of particles and spin configuration. The purple + signs correspond to the excitation energy of the main peak of the dynamic structure function.

not exactly known. In these situations there are useful theorems that allow us to compute M_n using only ground state properties [43]. These relations are named sum rules.

We can express these sum rules as [22]

$$(6.1.6) \qquad \begin{aligned} M_1 &= \frac{4}{N} \langle V_{\text{ho}} \rangle \\ M_3 &= \frac{4}{N} \left(\langle T \rangle + 3 \langle V_{\text{ho}} \rangle \right). \end{aligned}$$

In Fig. 6.3 we report the energy momenta M_{-1}, M_1 and M_3 as a function of the interaction strength. The sum rule M_{-1} has been calculated only using the explicit values of the dynamic structure function. For M_1 and M_3, the two methods, direct integration of the dynamic structure function and sum rules, are in perfect agreement for the case of two particles. For $N = 4$ the agreement between both methods is also very good. In all cases, the three momenta considered grow monotonically as the interaction strength is increased.

The sum rules can be used to obtain approximate values of the excitation energy. Indeed, if only one peak appears in the dynamic structure function, we can compute its excitation energy by $\sqrt{M_n/M_{n-2}}$ [43]. In a more general case this ratio can be used as an estimation of the energy

of the main peak.

In Fig. 6.4 we report the ratios $\sqrt{M_1/M_{-1}}$, $\sqrt{M_3/M_1}$ and excitation energy of the main contribution, associated to an intrinsic excitation, as a function of the interaction strength. We can observe that in the case of two particles, both estimations, $\sqrt{M_1/M_{-1}}$ and $\sqrt{M_3/M_1}$, differ and neither have the same energy than the intrinsic one, indicating that there is more than one peak in the dynamic structure function. These differences are bigger in the low and intermediate interacting regime, specially where the main excitation have the lowest energy. In the large interaction regime, the estimations provided by the ratios become closer to the excitation energy of the main intrinsic peak. This is because in the strongly interacting regime only one peak appears, similarly to the non-interacting case, as we have seen in Fig. 6.1. Nevertheless, when the number of particles increases, the two ratios provide closer estimates which in turn are close to the main intrinsic excitation energy. This can be seen in Fig. 6.2, where the intrinsic excitation is clearly dominant over the rest of excitations. Similar to the two particle case, the interaction strength region where the estimates are worse is where the intrinsic excitation energy takes its lower value.

6.2 Interaction quench

An alternative way to explore the internal excitations of an interacting many-body system is by performing an instantaneous quench of the interaction strength. In current experiments in ultracold atomic gases this is feasible. Indeed, a great control on the interaction strength is achieved by means of Feshbach resonances [10].

The system is prepared in the ground state, then the interaction strength is suddenly changed and as a consequence the original state is non-stationary anymore and evolves in time, populating the new set of eigenstates corresponding to the new value of the interaction strength.

This way to probe the system has similarities with the breathing mode. It also preserves spin and parity. However, due to the invariance of the interaction under translations, there are not center of mass excitations.

6.2.1 Time evolution of the perturbated system

We want to study the time evolution of the ground state corresponding to a given value of g after performing a sudden quench of the interaction strength to a new value g_{new}. The initial ground state is not anymore the ground state of the new Hamiltonian. However we can express the old ground state in terms of the eigenvectors of the new Hamiltonian and easily calculate its time

evolution:

$$(6.2.1) \qquad |\Psi(t=0)\rangle = \sum_n c_n |\Psi'_n\rangle,$$

where $|\Psi(t=0)\rangle$ is the ground state of the Hamiltonian before the quenching, and the states $|\Psi'_n\rangle$ are the eigenfunctions of the Hamiltonian after the quenching

$$(6.2.2) \qquad H' |\Psi'_n\rangle = E'_n |\Psi'_n\rangle,$$

with eigenenergies E'_n. The coefficients c_n can be computed as:

$$(6.2.3) \qquad c_n = \langle \Psi'_n |\Psi(t=0)\rangle.$$

The time evolution of the state after the quenching is calculated by taking into account that the states $|\Psi'_n\rangle$ are the eigenstates of the new Hamiltonian,

$$(6.2.4) \qquad |\Psi(t)\rangle = \sum_n c_n e^{-iE'_n t} |\Psi'_n\rangle.$$

In turn, the eigenstates $|\psi'_n\rangle$ can be expressed in terms of the many-body basis used to describe our system:

$$(6.2.5) \qquad |\Psi'_n\rangle = \sum_i C_{n,i} |\psi_i\rangle,$$

where $|\psi_i\rangle$ is a state of the many-body basis.

Knowing the time dependence of the state we can study the time dependence of any observable. In particular we are going to consider the time evolution of the central density of our system:

$$(6.2.6) \qquad \rho(x=0,t) = \sum_{i,j} \sum_{k,l} \sum_{n,m} c_n^* c_m e^{-i(E'_m - E'_n)t} C_{n,k}^* C_{m,l} \langle \psi_k | a_j^\dagger a_i | \psi_l \rangle \Phi_i^*(0)\Phi_j(0),$$

where $\Phi_i(x)$ are the single-particle harmonic oscillator wave functions. Notice that the time evolution of the system is governed by $E'_m - E'_n$, involving all energy differences of the states of the new Hamiltonian that have non-zero overlap with the ground-state of the old Hamiltonian. Also important is to realize that the relevance of a given frequency $2\pi\nu_{n,m} = E_n - E_m$ depends on the product of the projection coefficients $c_n^* c_m$.

For instance, it is plausible to think that, for a small change of g, the original ground state will have a large overlap with the new one. In this situation the dominant frequencies will be asociated to the differences $E'_n - E'_0$. In this sense, the frequencies would be similar to the frequencies involved in the calculation of the dynamical structure function associated to the breathing mode of H', with the exception that the excitations of the center of mass are not present.
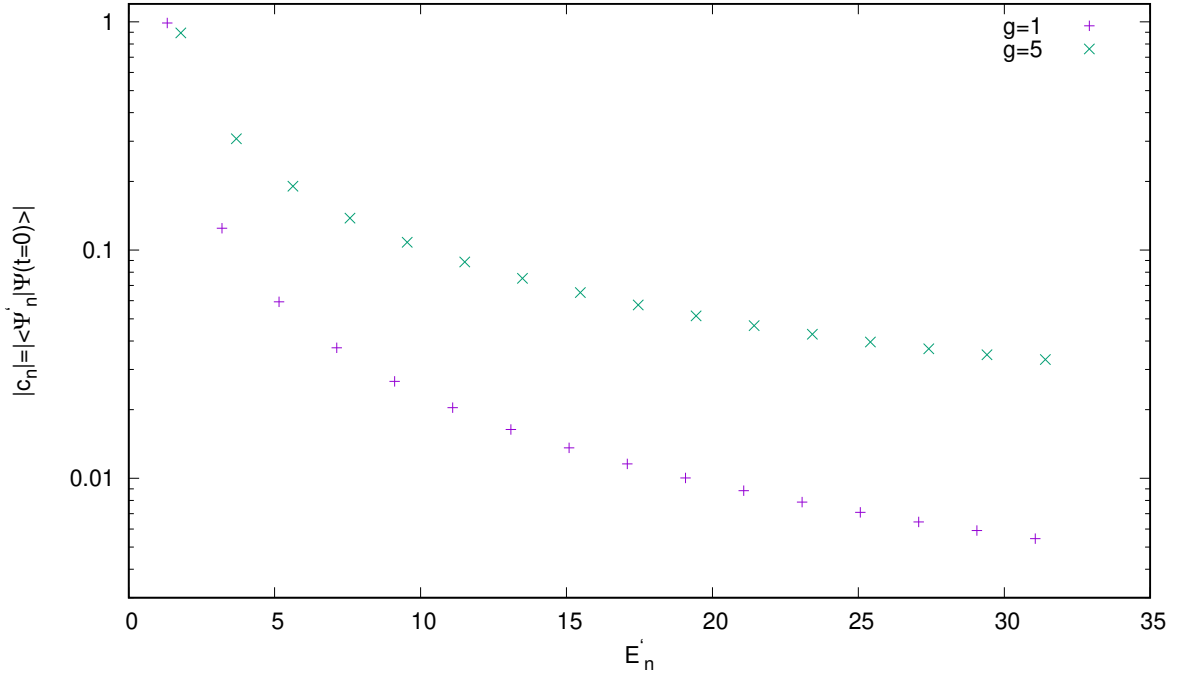
Figure 6.5: Projection of the initial ground state with $g = 0$ in the eigenstates of $g = 1$ and $g = 5$ as a function of its energy, for the system with two particles and zero total spin projection. The y axis is in logarithmic scale.

In Fig. 6.5, we report the projections of the ground state of the non-interacting system to the eigenstates of $H'(g = 1)$. In this quench, the interaction strength suffers a sudden change from $g = 0$ to $g = 1$. We also report the projection for the quench $g = 0 \rightarrow 5$. Notice that not all the eigenstates are populated, one should consider only projections to states of H' with the same parity and total and third spin component and with the same center of mass state in the initial and final states. In the case $g = 1$ (small g) there is a dominant projection into the ground state of H' and then the value of the projections decrease rather quickly. For the case $g = 5$, the largest projection is smaller than in the previous case but the projections to higher states decrease more slowly. Therefore for $g = 5$ one has relevant projections to higher excited states.

6.2.2 Central density oscillations

In this section we propose a method to determine the low energy spectrum of a trapped few-body system, by applying a sudden quench of the strength of the interatomic interactions. In principle, the procedure can be implemented experimentally.

One can prepare a system with N particles trapped in a harmonic potential without inter-actions. Then apply to the system a sudden quench of the interaction, let the system evolve
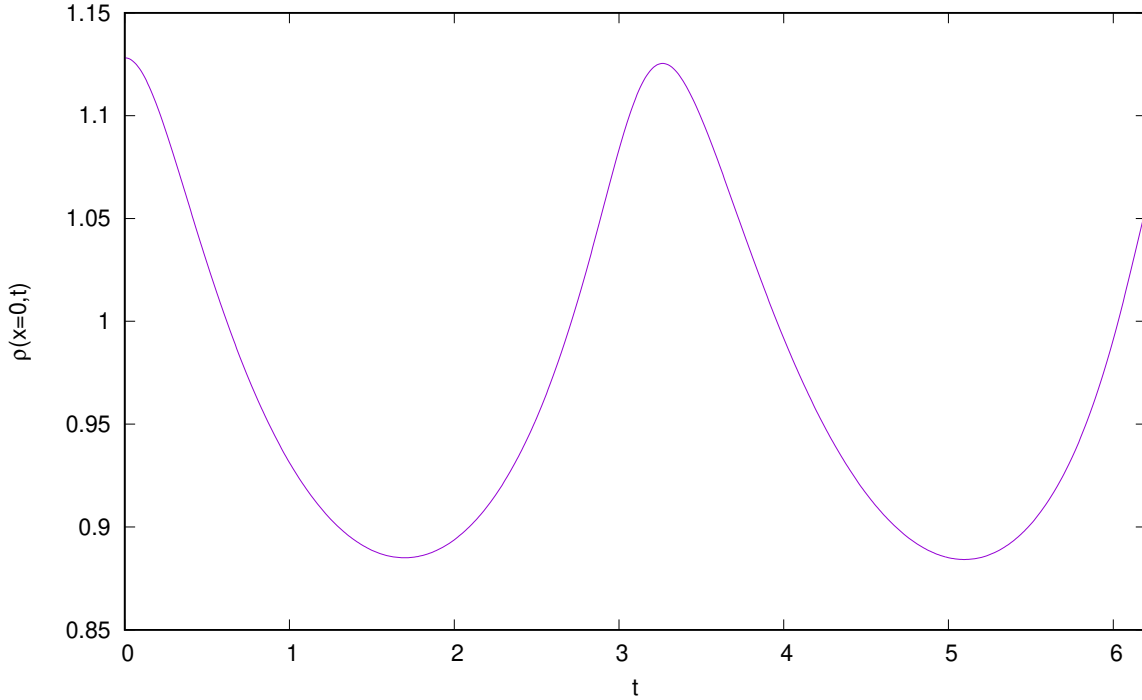
Figure 6.6: Central density of a two particle system as a function of time after a quench of the interaction strength from $g = 0 \rightarrow 1$.

and measure the central density as a function of time. One should observe an oscillatory behavior.

In Fig. 6.6 we report the theoretical prediction of the central density as a function of time after a quench of the interaction strength from $g = 0 \rightarrow 1$ for the two particle case. At $t = 0$ the central density takes the value of the central density for the non-interacting case, shown on Fig. 4.3. Then the central density follows an oscillatory behavior. Notice that at the beginning the central density decreases and has a minimum due to the fact that the particles feel the repulsive interaction and tend to be more delocalized.

In order to obtain information on the energy spectrum of the system at $g = 1$ (the final value of the quench), we need to perform a Fourier analysis of the central density as a function of time. In this way one obtains the characteristic oscillation frequencies which in turn are related to the differences of the energies of the system for $g = 1$. Therefore, with the frequencies one has access to the excitation energies $\Delta E = 2\pi\nu$. To extract the frequencies by the Fourier analysis one needs to know the time evolution of the central density in a interval of time longer than the one shown in the Fig. 5.6. Notice that it is convenient to subtract the average value of the central density in order to avoid a peak with zero frequency in the Fourier analysis. Actually, this peak at $\nu = 0$ does not provide any physical information about the energy spectrum and could overlap with other
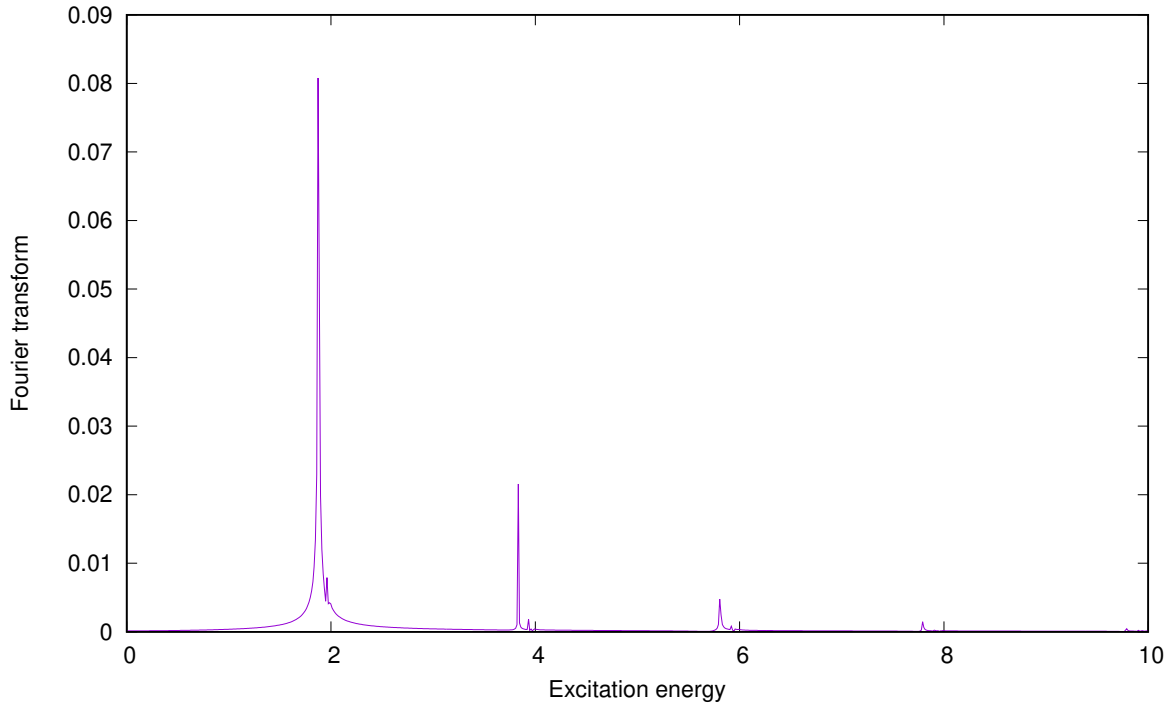
Figure 6.7: Excitation energies obtained from the frequencies associated to the Fourier analysis of the central density as a function of time, after a quench of the interaction strength from $g = 0 \rightarrow 1$.

peaks at low frequencies.

In Fig. 6.7, we report the excitation energies corresponding to the oscillation frequencies obtained by the Fourier analysis of the time dependence of the central density of the two particle system after a quench of the interaction form $g = 0 \rightarrow 1$. We observe a dominant peak at low energy, and more peaks with smaller intensity at higher energies. This frequency analysis is done using a large interval of time and the average value of the central density is subtracted before doing the frequency analysis.

The location of the peaks, allows to recover the excitation energies of the low excited states respect to the ground state corresponding to $g = 1$. However, to find the absolute energies of these states would be necessary to have access also to the ground-state energy of the system.

The figure reveals the existence of a dominant peak at an excitation energy a little smaller than 2, and other two main visible peaks at energies a little smaller than 4 and 6, with much smaller strength. All these peaks correspond to energy differences of the first excited states, which have non-zero overlap with the non-interacting ground state ($g = 0$), and the ground state of the system corresponding to $g = 1$, respectively. Notice that due to the reentrance phenomena,

47

discussed in the previous section, the excitation energies are a little smaller than 2,4, and 6 respectively. It is also worth to mention the existence of a smaller but distinguishable peak, very close to the excitation energy 2, that corresponds to the difference between the third and the second excited states (see Fig. 6.7).

SUMMARY AND CONCLUSIONS

In this thesis we have considered a 1D gas of ultracold 1/2 spin fermions trapped in a harmonic oscillator potential. The fermions interact through a contact interaction that, due to the Pauli principle, is active only between particles with opposite spin. This type of systems has already been realized experimentally and new experiments concerning the structure and mainly the dynamics are expected for the near future. Our main objective has been to study both static and dynamic properties of the system as a function of the interaction strength. This interaction can be controlled experimentally by means of Feshbach resonances.

In the first chapter, we have described the Hamiltonian of the system, that includes both the harmonic oscillator confining potential and the interaction between the fermions. Furthermore, two analytical limits have been discussed in detail: the non-interacting and the infinite interacting limits. In both cases, the many-body wave function, the energy and the density profile of the ground state have been derived. In addition, the second quantization formalism has been introduced as the framework for the calculation of the Hamiltonian.

In the second chapter, we have presented the method that we use to compute the energy spectrum and the wave functions: exact diagonalization. In addition, we have described the systems that we study: how many particles and which spin projection we consider. Then we have introduced an efficient method to diagonalize the Hamiltonian, by considering only single-particle states producing non-interacting many-body basis states with less than a given energy. These states define the Hilbert subspace where we diagonalize the matrix Hamiltonian. Using this procedure one can get accurate results for the low part of the spectrum using subspaces with much smaller dimensionality and therefore taking much less time to diagonalize the Hamiltonian. In this

line, we also developed a useful method that allows to compute the interaction matrix elements involving high-order Hermite polynomials. This methods is based in the use of logarithms to avoid the numerical problems caused by factorials. At the end of the chapter, we have performed a benchmark calculation of the two-particle system by comparing our numerical calculations and the analytical results. This comparison shows that the calculations are more accurate for the repulsive regime of the interaction.

In the third chapter, we studied several static properties of the ground state of the system, mainly the total energy and their contributions. The energy contributions have been used to check the fulfillment of the virial relation, obtaining very good results for repulsive interaction, specially in the low-interacting regime. The fulfilment of the virial relation reinforced the consistency of the calculations. We also study the density profile of the ground state. In the non-interacting and the infinite interacting cases our calculations are in perfect agreement with the analytical results presented in the first chapter. In the next step, we have computed the natural orbits and its eigenvalues. Their analysis reveals the presence of correlations in the system when the interaction is turned on. The existence of correlations has motivated the study of the entanglement of the system. In our case, we have studied the entanglement entropy between one spin-down particle and the rest, all with spin up. In this situation, we obtained that for the non-interacting case, the entanglement entropy is zero, but when the interaction is turned on, the entanglement entropy increases indicating the presence of correlations.

In the fourth chapter we have presented the energy spectrum of different systems and we have explicitly wrote the wave function for some of them in the non-interacting and infinite interacting limits. In addition, we have presented a method to assign total spin to the states, without an explicit calculation. It is based in the comparison of the energy spectrum for different third spin component for the same number of particles and detecting the degeneracies. In the same way, we presented a method to identify the parity of each state without the explicit calculation.

In the last chapter, we have studied several dynamic properties. First we have studied the perturbation of a mono-polar excitation over the ground state, in order to excite the breathing mode. We have computed the dynamic structure function associated to this perturbation, and using the knowledge of the energy spectra obtained in the previous chapter, we have identify the excited states. The parity and spin assignation in the previous chapter was useful to identify the excited states by the breathing mode. We have also calculated the energy momenta (M_n) associated to the dynamic structure function and we use the ratios $\sqrt{M_n/M_{n-2}}$ to estimate the average excitation energies. The differences between the ratios $\sqrt{M_n/M_{n-2}}$ for different n indicates the existence of more than one excited state in the dynamic structure function. In fact, for the two particle case there is more than one dominant peak in the response of the system.

However, for larger number of particles, even if there are more excited states, the strength of the response is concentrated in one dominant peak.

Finally, we have studied the effect of a quench of the interaction strength on the system. We have discussed the similarities and the differences between the quench and the breathing mode. In addition, we have proposed an experimental procedure to measure the excitation energies based on the measurement of the time evolution of the central density of the system after a quench of the interaction. Analyzing the frequencies of the Fourier transform of the time dependence of the oscillation of the central density after the quench one can obtain information about the excitation energies

THE TWO-BODY MATRIX ELEMENTS OF THE INTERACTION

The evaluation of the two-body interaction matrix elements Eq.(2.3.10), requires the calculation of an integral with four wave functions.

$$
\begin{aligned}
(A.0.1) \qquad v_{ij,kl} &= g\delta_{m_i,m_k}\delta_{m_j,m_l}\int dx\Phi_i^*(x)\Phi_j^*(x)\Phi_k(x)\Phi_l(x)\\
&= g\delta_{m_i,m_k}\delta_{m_j,m_l}I_{ijkl}
\end{aligned}
$$

The integral I_{abcd} can be solved analytically, because the wave functions are the harmonic oscillator wave functions Eq.(2.1.4),

$$
\begin{aligned}
(A.0.2) \qquad I_{abcd} &= \int_{-\infty}^{\infty}\Phi_a(x)\Phi_b(x)\Phi_c(x)\Phi_d(x)dx\\
&= \frac{1}{\pi\sqrt{2^{a+b+c+d}a!b!c!d!}}\int_{\infty}^{\infty}e^{-2x^2}H_a(x)H_b(x)H_c(x)H_d(x)dx\,.
\end{aligned}
$$

Let us consider,

$$
(A.0.3) \qquad I'_{abcd} = \int_{-\infty}^{\infty}e^{-2x^2}H_a(x)H_b(x)H_c(x)H_d(x)dx\,.
$$

We notice that this integral has to be zero if $(a+b+c+d)$ is an odd number. This is because the Φ_i wave functions have well defined parity. Therefore if the multiplication of the four functions is odd, the integral value will be zero. This is why we only calculate the integrals with $(a+b+c+d)$ even.

Using the properties [44]

$$
\begin{aligned}
(A.0.4) \qquad \int_{-\infty}^{\infty}&e^{-2x^2}H_a(x)H_b(x)H_c(x) =\\
&= \frac{2^{(a+b+c-1)/2}}{\pi}\Gamma\left(\frac{a+b-c+1}{2}\right)\Gamma\left(\frac{a-b+c+1}{2}\right)\Gamma\left(\frac{-a+b+c+1}{2}\right),
\end{aligned}
$$

and

(A.0.5) $$H_m(x)H_n(x) = 2^n n! \sum_{r=0}^{n} \frac{m!}{(n-r)!(m-n+r)!} \frac{H_{m-n+2r}(x)}{2^r r!}, n \leq m.$$

We can express the integral I'_{abcd} as

(A.0.6)
$$\begin{aligned} I'_{abcd} =& 2^d d! \sum_{r=0}^{d} \frac{c!}{(d-r)!(c-d+r)!} \frac{1}{2^r r!} \frac{2^{(a+b+c-d+2r-1)/2}}{\pi} \\ & \times \Gamma\left(\frac{a+b-c+d+1}{2} - r\right) \Gamma\left(\frac{a-b+c-d+1}{2} + r\right) \\ & \times \Gamma\left(\frac{-a+b+c-d+1}{2} + r\right), \end{aligned}$$

Notice that the arguments of the gamma functions (Γ) are half-integers. Because $(a+b+c+d)$ is even, then when changing any sign, the result will remain even, and the gamma functions read,

(A.0.7)
$$\left.\begin{aligned} \Gamma\left(n + \frac{1}{2}\right) &= \sqrt{\pi}\frac{(2n)!}{2^n n!} \\ \Gamma\left(\frac{1}{2} - n\right) &= \sqrt{\pi}\frac{(-4)^n n!}{(2n)!} \end{aligned}\right\}, n \geq 0$$

Finally, the integral I_{abcd} can be expressed as

(A.0.8)
$$\begin{aligned} I_{abcd} =& \frac{1}{\pi^2\sqrt{2}} \sqrt{\frac{c!d!}{a!b!}} \sum_{r=0}^{d} \frac{1}{r!(d-r)!(c-d+r)!} \Gamma\left(\frac{a+b-c+d+1}{2} - r\right) \\ & \times \Gamma\left(\frac{a-b+c-d+1}{2} + r\right) \Gamma\left(\frac{-a+b+c-d+1}{2} + r\right), \end{aligned}$$

DERIVATION OF THE VIRIAL THEOREM

The energy of the system is given by the expectation values $\langle E \rangle = \langle T \rangle + \langle V_{\text{ho}} \rangle + \langle V_{\text{int}} \rangle$, where the operators are defined as

(B.0.1)
$$T = \sum_i -\frac{1}{2}\frac{\partial^2}{\partial x_i^2} \, , \, V_{\text{ho}} = \sum_i \frac{x_i^2}{2} \, , \, V_{\text{int}} = \sum_{j<i} g\delta(x_i - x_j).$$

We use the virial theorem to obtain a relation between the different energy contributions. The virial theorem is based on a scaling transformation of the many-body wave function and the transformation of the different energy contribution under the scaling transformations. We start by defining a wave function

(B.0.2)
$$\Psi_\lambda(x_1, x_2, ..., x_N) = \lambda^{N/2}\Psi(x_1, x_2, ..., x_N).$$

This wave function has the same normalization than Ψ.

First, we compute the transformation of the kinetic energy,

(B.0.3)
$$\begin{aligned}
\langle T(\lambda)\rangle &= \langle \Psi_\lambda | \sum_i -\frac{1}{2}\frac{\partial^2}{\partial x_i^2} |\Psi_\lambda\rangle \\
&= -N\frac{1}{2}\lambda^N \int dx_1 dx_2 ... dx_N \Psi^*(\lambda x_1, ..., \lambda x_n)\frac{\partial^2}{\partial x_1^2}\Psi(\lambda x_1, ..., \lambda x_n) \\
&= -N\frac{1}{2}\lambda^N \int \frac{1}{\lambda^N} dy_1 dy_2 ... dy_N \Psi^*(y_1, ..., y_n)\lambda^2 \frac{\partial^2}{\partial y_1^2}\Psi(y_1, ..., y_n) \\
&= \lambda^2 \langle T(\lambda = 1)\rangle .
\end{aligned}$$

The harmonic oscillator energy transformation is

$$
\begin{aligned}
\langle V_{\text{ho}}(\lambda) \rangle &= \langle \Psi_\lambda | \sum_i \frac{x_i^2}{2} | \Psi_\lambda \rangle \\
&= N\frac{1}{2}\lambda^N \int dx_1 dx_2 ... dx_N \Psi^*(\lambda x_1, ..., \lambda x_n) x_1^2 \Psi(\lambda x_1, ..., \lambda x_n) \\
&= N\frac{1}{2}\lambda^N \int \frac{1}{\lambda^N} dy_1 dy_2 ... dy_N \Psi^*(y_1, ..., y_n)\lambda^{-2} y_1^2 \Psi(y_1, ..., y_n) \\
&= \lambda^{-2} \langle V_{\text{ho}}(\lambda = 1) \rangle \, .
\end{aligned}
$$

(B.0.4)

And finally, the interaction energy transformation is

$$
\begin{aligned}
\langle V_{\text{int}}(\lambda) \rangle &= \langle \Psi_\lambda | \sum_{j<i} g\delta(x_i - x_j) | \Psi_\lambda \rangle \\
&= \frac{N(N-1)}{2} g\lambda^N \int dx_1 dx_2 ... dx_N \Psi^*(\lambda x_1, ..., \lambda x_n)\delta(x_2 - x_1)\Psi(\lambda x_1, ..., \lambda x_n) \\
&= N\frac{N(N-1)}{2} g\lambda^N \int \frac{1}{\lambda^N} dy_1 dy_2 ... dy_N \Psi^*(y_1, ..., y_n)\lambda\delta(y_2 - y_1)\Psi(y_1, ..., y_n) \\
&= \lambda \langle V_{\text{int}}(\lambda = 1) \rangle \, .
\end{aligned}
$$

(B.0.5)

The expectation value of the Hamiltonian with the scaled wave function can be written as

(B.0.6)
$$
\langle E_\lambda \rangle = \langle \Psi_\lambda | H | \Psi_\lambda \rangle = \lambda^2 \langle T(\lambda = 1) \rangle + \lambda^{-2} \langle V_{\text{ho}} \rangle + \lambda \langle V_{\text{int}} \rangle \, ,
$$

and taking into account that at $\lambda = 1$ the energy has a stationary point, i.e.,

(B.0.7)
$$
\frac{\partial \langle E_\lambda \rangle}{\partial \lambda} \bigg|_{\lambda=1} = 0 \, ,
$$

we derive the virial relation

(B.0.8)
$$
\begin{aligned}
\frac{\partial \langle E_\lambda \rangle}{\partial \lambda} \bigg|_{\lambda=1} &= 0 = 2\lambda \langle T(\lambda = 1) \rangle + -2\lambda^{-3} \langle V_{\text{ho}}(\lambda = 1) + \langle V_{\text{int}}(\lambda = 1) \rangle \big|_{\lambda=1} \\
&= 2\langle T \rangle - 2\langle V_{\text{ho}} \rangle + \langle V_{\text{int}} \rangle = 0 \, .
\end{aligned}
$$

In order to compute the expectation values of the different operators, it is useful to derive its expression in second quantization.

The states of the single-particle basis are

(B.0.9)
$$
|n\rangle = \frac{1}{\sqrt{2^n n! \sqrt{\pi}}} H_n(x) e^{-x^2/2} |\chi_{m_n}\rangle = A_n H_n(x) e^{-x^2/2} |\chi_{m_n}\rangle \, ,
$$

where A_n is a normalization constant, which depends on n. On the other hand $|\chi_m\rangle$ is a single-particle spin-1/2 wave function, with spin projection m.

In order to operate with the Hermite polynomials, we use the following properties:
The m-th derivative of a Hermite polynomial,

$$(B.0.10) \qquad H_n^{(m)} = 2^m \frac{m!}{(n-m)!} H_{n-m}(x),$$

the recurrence relation,

$$(B.0.11) \qquad H_{n+1}(x) = 2x H_n(x) - 2n H_{n-1}(x),$$

the orthogonality of the Hermite polynomials

$$(B.0.12) \qquad \int_{-\infty}^{\infty} H_m(x) H_n(x) e^{-x^2} = \delta_{m,n} 2^n n! \sqrt{\pi},$$

the n-th power of x expressed in terms of Hermite polynomials

$$(B.0.13) \qquad x^n = \frac{n!}{2^n} \sum_{m=0}^{n/2} \frac{1}{m!(n-2m)!} H_{n-2m},$$

and the product of two Hermite polynomials as a function of the sum of Hermite polynomials

$$(B.0.14) \qquad H_m(x) H_n(x) = 2^n n! \sum_{r=0}^{n} \frac{m!}{(n-r)!(m-n+r)!} \frac{H_{m-n+2r}(x)}{2^r r!}, n \le m.$$

First, we derive the expression of the one-body harmonic oscillator matrix elements, that reads,

$$(B.0.15) \qquad \langle j | V_{\mathrm{ho}} | i \rangle = \langle j | \frac{x^2}{2} | i \rangle,$$

ssing Eq.(B.0.13) we can write x^2 as

$$(B.0.16) \qquad x^2 = \frac{1}{2} \left(\frac{1}{2} H_2 + H_0 \right).$$

Then, writing explicitly the Eq.(B.0.15), and taking into account Eq.(B.0.14) and the orthogonality Eq.(B.0.12) we get,

(B.0.17)

$$\langle j | V_{\mathrm{ho}} | i \rangle = \langle j | \frac{1}{4} \left(\frac{1}{2} H_2 + H_0 \right) A_i H_i e^{-x^2/2} | \chi_{m_i} \rangle$$
$$= \langle j | \frac{A_i}{4} \left(2n(i-1) H_{i-2} + (2i+1) H_i + \frac{1}{2} H_{i+2} \right) e^{-x^2/2} | \chi_{m_i} \rangle$$
$$= \frac{A_i A_j}{4} \int dx H_j(x) \left(2n(i-1) H_{i-2}(x) + (2i+1) H_i(x) + \frac{1}{2} H_{i+2}(x) \right) e^{-x^2} \langle \chi_{m_i} | \chi_{m_j} \rangle.$$

Finally, the harmonic oscillator energy is

$$(B.0.18) \qquad \langle j | V_{\mathrm{ho}} | i \rangle = \frac{1}{4} \left(\sqrt{i(i-1)} \delta_{j,i-2} + (2i+1) \delta_{j,i} + \sqrt{(i+2)(i+1)} \delta_{j,i+2} \right) \delta_{m_i,m_j}.$$

Now, we derive the expression of the one-body kinetic matrix elements, that read,

$$(\text{B.0.19}) \qquad \langle j| T |i\rangle = \langle j| \left(-\frac{1}{2}\frac{\partial^2}{\partial x^2} \right) |i\rangle .$$

Taking the first and second derivatives of the harmonic oscillator wave function and using the Eq.(B.0.10)

$$(\text{B.0.20}) \qquad \frac{\partial}{\partial x} H_n(x) = 2n H_{n-1}(x),$$

$$(\text{B.0.21}) \qquad \frac{\partial^2}{\partial x^2} H_n(x) = 4n(n-1) H_{n-2}(x),$$

we can express the kinetic energy as

$$(\text{B.0.22}) \qquad \langle j| T |i\rangle = \langle j| \frac{A_i}{2} e^{-x^2/2} \left(-4i(i-1)H_{i-2} + 4xi H_{i-1} + H_i - x^2 H_i \right) \big| \chi_{m_i} \big\rangle .$$

Using Eq.(B.0.11) we obtain:

$$(\text{B.0.23}) \qquad \langle j| T |i\rangle = \langle j| A_i e^{-x^2/2} \left(i + \frac{1}{2} - \frac{x^2}{2} \right) H_i(x) \big| \chi_{m_i} \big\rangle ,$$

and taking the results of the harmonic oscillator potential energy Eq.(B.0.18), the kinetic energy matrix elements are expressed as

$$(\text{B.0.24}) \qquad \langle j| T |i\rangle = \frac{1}{4} \left(-\sqrt{i(i-1)}\delta_{j,i-2} + (2i+1)\delta_{j,i} - \sqrt{(i+2)(i+1)}\delta_{j,i+2} \right) \delta_{m_i,m_j} .$$

[1] L. P. Kouwenhoven, D. G. Austing and S. Tarucha, "*Few-electron quantum dots*", Rep. Prog. Phys. **64**, 701 (2001).

[2] F. E. Close, "*An introduction to quarks and partons*", Academic Press (1979).

[3] H.-W. Hammer, A. Nogga, and A. Schwenk, "*Three-body forces: From cold atoms to nuclei*", Rev. Mod. Phys. **85**, 197 (2013).

[4] M. H. Anderson, J. R. Ensher, M. R. Matthews, C. E. Wieman, and E. A. Cornell, "*Observation of Bose-Einstein Condensation in a Dilute Atomic Vapor*", Science **269**, 198 (1995).

[5] K. B. Davis, M.-O. Mewes, M. R. Andrews, N. J. van Druten, D. S. Durfee, D. M. Kurn, and W. Ketterle "*Bose-Einstein Condensation in a Gas of Sodium Atoms*", Phys. Rev. Lett. **75**, 3969 (1995).

[6] A. G. Truscott, K. E. Strecker, W. I. McAlexander, G. B. Partridge, and R. G. Hulet, "*Observation of Fermi Pressure in a Gas of Trapped Atoms*", Science **291**, 2570 (2001).

[7] P. Cheiney, C.R. Cabrera, J. Sanz, B. Naylor, L. Tanzi, and L. Tarruell, "*Bright Soliton to Quantum Droplet Transition in a Mixture of Bose-Einstein Condensates*", Phys. Rev. Lett. **120**, 135301 (2018).

[8] F. Serwane, G. Zürn, T. Lompe, T. B. Ottenstein, A. N. Wenz, and S. Jochim, "*Deterministic preparation of a tunable few-fermion system*", Science **332**, 336 (2011).

[9] E. Haller, M. Gustavsson, M. J. Mark, J. G. Danzl, R. Hart, G. Pupillo, and H.-C. Nagerl, "*Realization of an Excited, Strongly Correlated Quantum Gas Phase*", Science **325**, 1224 (2009).

[10] C. Chin, R. Grimm, P. Julienne, and E. Tiesinga, "*Feshbach Resonances in Ultracold Gases*", Rev. Mod. Phys. **82**, 1225 (2010).

[11] W. S. Bakr, J. I. Gillen, A. Peng, S. Fölling, and M. Greiner, "*A quantum gas microscope for detecting single atoms in a Hubbard-regime optical lattice*", Nature **462**, 74 (2009).

[12] I. Bloch, "*Ultracold quantum gases in optical lattices*", Nat. Phys. **1**, 23 (2005).

[13] L. Tanzi, E. Lucioni, F. Famà, J. Catani, A. Fioretti, C. Gabbanini, R. N. Bisset, L. Santos, and G. Modugno, "*Observation of a dipolar quantum gas with metastable supersolid properties*", Phys. Rev. Lett. **122**, 130405 (2019).

[14] I. Bloch, J. Dalibard, and W. Zwerger, "*Many-Body Physics with Ultracold Gases*", Rev. Mod. Phys. **80**, 885 (2008).

[15] T. Sowinski and M. A. Garcia-March "*One-dimensional mixtures of several ultracold atoms: a review*", Rep. Prog. Phys. **82**, 104401 (2019).

[16] E. K. Laird, Z.-Y. Shi, M. M. Parish, and J. Levinsen, "*SU(N) fermions in a one-dimensional harmonic trap*", Phys. Rev. A **96**, 032701 (2017).

[17] M. C. Gordillo, "*One-dimensional harmonically confined SU(N) fermions*", Phys. Rev. A **100**, 023603 (2019).

[18] T. Sowinski, T. Grass, O. Dutta, and M. Lewenstein "*Few interacting fermions in one-dimensional harmonic trap*", Phys. Rev. Lett. **102**, 160402 (2009).

[19] M. Pyzh, S. Kronke, C. Weitenberg, and P. Schmelcher, "*Spectral properties and breathing dynamics of a few-body Bose-Bose mixture in a 1D harmonic trap*", New J. Phys. **20**, 015006 (2018).

[20] M. Olshanii, "*Atomic scattering in the presence of an external confinement and a gas of impenetrable bosons*", Phys. Rev. Lett. **81**, 938 (1998).

[21] Q. Hummel, J. Diego Urbina, and K. Richter, "*Partial Fermionization-Spectral Universality in 1D Repulsive Bose Gases*", Phys. Rev. Lett. **122**, 240601 (2019).

[22] D. Ledesma, A. Romero-Ros, A. Polls, and B. Julià-Diaz, "*Dynamic structure function of two interacting atoms in 1D*", arXiv:1811.01790 (2018).

[23] X. Y. Yin, Y. Yan, and D. Hudson Smith, "*Dynamics of small trapped one-dimensional Fermi gas under oscillating magnetic fields*", Phys. Rev. A. **94**, 043639 (2016).

[24] L. Guan, S. Chen, Y. Wang, and Z. Ma "*Exact solution for infinitely strongly interacting Fermi gases in tight waveguides*", Phys. Rev. Lett. **102**, 160402 (2009).

[25] E. H. Lieb and D. Mattis, "*Theory of ferromagnetism and the ordering of electronic energy levels*", Phys. Rev. **125**, 164 (1962).

[26] W.H. Dickhoff and D. Van Neck, *M*any-Body Theory Exposed! , World Scientific, Singapore, (2008).

[27] T. Busch, B.G. Englert, K. Rzazewski, and M. Wilkens, "*Two cold atoms in an harmonic trap*", Foundations of Physics **28**, 549 (1998).

[28] K. Wu and H. Simon, "*Thick-restart Lanczos method for large symmetric eigenvalue problems*", SIAM J. Matrix Anal. Appl. **22**, 602 (2000).

[29] D. Raventos, T. Grass, M. Lewenstein, and B. Julià-Diaz, "*Cold bosons in optical lattices: a tutorial for Exact Diagonalization*", Phys. B: At. Mol. Opt. Phys. **50**, 113001 (2017).

[30] M. Plodzien, D. Wiater, A. Chrostowski, and T. Sowinski, "*Numerically exact approach to few-body problems far from a perturbative regime*", arXiv:1803.08387.

[31] T. Grining, M. Tomza, M. Lesiuk, M. Przybytek, M. Musial, P. Massignan, M. Lewenstein, and R. Moszynski, "*Many interacting fermions in a one-dimensional harmonic trap: a quantum-chemical treatment*", New J. Phys. **17**, 115001 (2015).

[32] M. Girardeau, "*Relationship between Systems of Impenetrable Bosons and Fermions in One Dimension* ", J. Math. Phys. **1**, 516 (1960).

[33] H. M. Wiseman1 and J. A. Vaccaro, "*Entanglement of Indistinguishable Particles Shared between Two Parties*", Phys. Rev. Lett. **91**, 097902 (2003).

[34] A. M. Gavrilik and Yu. A. Mishchenko, "*Entanglement entropy of composite fermions realized by (deformed) fermions vs. that of composite bosons*", arXiv:1504.00529 (2015).

[35] A. M. Kaufman, B. J. Lester, M. Foss-Feig, M. L. Wall, A. M. Rey, and C. A. Regal, "*Entangling two transportable neutral atoms via local spin exchange*", Nature **527**, 208 (2015).

[36] A. N. Wenz, G. Zürn, S. Murmann, I. Brouzos, T. Lompe, and S. Jochim, "*From Few to Many: Observing the Formation of a Fermi Sea One Atom at a Time*", Science **342**, 6157 (2013).

[37] X. Li, D. Pecak, T. Sowinski, J. Sherson, and A. E. B. Nielsen, "*Global optimization for quantum dynamics of few-fermion systems*", Phys. Rev. A **97**, 033602 (2018).

[38] B. Fang, G. Carleo, and I. Bouchoule, "*Quench-induced breathing mode of one-dimensional Bose gases*", Phys. Rev. Lett. **113**, 035301 (2014).

[39] C. Menotti and S. Stringari, "*Collective oscillations of a 1D trapped Bose gas*", Phys. Rev. A, **66**, 043610 (2002).

[40] H. Moritz, T. Stoferle, M. Kohl, and T. Esslinger, "*Exciting Collective Oscillations in a Trapped 1D Gas*", Phys. Rev. Lett. **91**, 250402 (2003).

[41] W. Kohn, "*Cyclotron Resonance and de Haas-van Alphen Oscillations of an Interacting Electron Gas*", Phys. Rev. **123**, 1242 (1961).

[42] A. Iu. Gudyma, G. E. Astrakharchik, and Mikhail B. Zvonarev, "*Reentrant behavior of the breathing-mode-oscillation frequency in a one-dimensional*", Phys. Rev. A **92**, 021601 (2015).

[43] O. Bohigas, A. M. Lane, and J. Martorell, "*Sum rules for nuclear collective excitations*", Phys. Rep. **51**, 267 (1979).

[44] E. C. Titchmarsh, "*Some integral Involving Hermite Polynomials*", J.London Math.Soc. **23**, 15 (1948).